

Geochemistry, Geophysics, Geosystems

RESEARCH ARTICLE

10.1029/2020GC009122

Key Points:

- Suite of paleobathymetric grids encompassing key time intervals in Southern Ocean development since the Eocene/Oligocene Boundary
- Detailed sediment isopachs reveal two distinct sedimentation surges in relation to the advancement of the Antarctic Ice Sheets
- Reconstruction of the Southern Ocean gateways point to the potential of deep-water exchange in the middle Oligocene

Supporting Information:

- Supporting Information S1
- Figure S1

Correspondence to:

K. Hochmuth,
Katharina.Hochmuth@awi.de;
kh355@leicester.ac.uk

Citation:









Hochmuth, K., Gohl, K., Leitchenkov, G., Sauermilch, I., Whittaker, J. M., Uenzelmann-Neben, G., et al. (2020). The evolving paleobathymetry of the circum-Antarctic Southern Ocean since 34 Ma: A key to understanding past cryosphere-ocean developments. *Geochemistry, Geophysics, Geosystems*, 21, e2020GC009122. <https://doi.org/10.1029/2020GC009122>

Received 20 APR 2020

Accepted 17 JUN 2020

Accepted article online 23 JUN 2020

The Evolving Paleobathymetry of the Circum-Antarctic Southern Ocean Since 34 Ma: A Key to Understanding Past Cryosphere-Ocean Developments

K. Hochmuth^{1,2} , K. Gohl¹ , G. Leitchenkov^{3,4} , I. Sauermilch⁵ , J. M. Whittaker⁵ , G. Uenzelmann-Neben¹ , B. Davy⁶ , and L. De Santis⁷ 

¹Alfred Wegener Institute Helmholtz-Centre for Polar and Marine Research, Bremerhaven, Germany, ²School of Geology, Geography and the Environment, University of Leicester, Leicester, UK, ³Department of Antarctic Geoscience, All Russia Scientific Research Institute for Geology and Mineral Resources of the Ocean, St. Petersburg, Russia, ⁴St. Petersburg State University, St. Petersburg, Russia, ⁵Institute for Marine and Antarctic Studies, University of Tasmania, Hobart, Australia, ⁶GNS Science, Lower Hutt, New Zealand, ⁷National Institute of Oceanography and Applied Geophysics, OGS, Trieste, Italy

Abstract The Southern Ocean is a key player in the climate, ocean, and atmospheric system. As the only direct connection between all three major oceans since the opening of the Southern Ocean gateways, the development of the Southern Ocean and its relationship with the Antarctic cryosphere has influenced the climate of the entire planet. Although the depths of the ocean floor have been recognized as an important factor in climate and paleoclimate models, appropriate paleobathymetric models including a detailed analysis of the sediment cover are not available. Here we utilize more than 40 years of seismic reflection data acquisition along the margins of Antarctica and its conjugate margins, along with multiple drilling campaigns by the International Ocean Discovery Program (IODP) and its predecessor programs. We combine and update the seismic stratigraphy across the regions of the Southern Ocean and calculate ocean-wide paleobathymetry grids via a backstripping method. We present a suite of high-resolution paleobathymetric grids from the Eocene-Oligocene Boundary to modern times. The grids reveal the development of the Southern Ocean from isolated basins to an interconnected ocean affected by the onset and vigor of an Antarctic Circumpolar Current, as well as the glacial sedimentation and erosion of the Antarctic continent. The ocean-wide comparison through time exposes patterns of ice sheet development such as switching of glacial outlets and the change from wet-based to dry-based ice sheets. Ocean currents and bottom-water production interact with the sedimentation along the continental shelf and slope and profit from the opening of the ocean gateways.

Plain Language Summary The Southern Ocean is the only ocean which connects all three major world's oceans and therefore plays a vital role in our planet's oceanographic and atmospheric systems. We reconstruct the changing depth and geometry of the Southern Ocean seafloor since the establishment of a major ice sheet in Antarctica (34 Ma). We also provide an inventory of ice-sheet eroded sediments deposited in the Southern Ocean, which has previously been highly underestimated. This ocean-wide study shows the development of the Southern Ocean from individual, separated basins into the home of the strong Circumpolar current system, by the deepening of the land bridges between Antarctica and Australia and Antarctica and South America. The sediments deposited in the Southern Ocean, especially along the Antarctic margin, illustrate the growth and retreat of the Antarctic ice sheets showing two distinct pulses of enhanced sedimentation at the first continental-scale glaciation of Antarctica (34 Ma) and after the warm phase of the Miocene Climatic Optimum. On a local and regional scale, we trace the amount of erosion provided by glacier systems along the Antarctic coast. The presented suite of seafloor grids will be made available to the geoscientific community and is an important additional input parameter for paleo-models.

©2020. The Authors.

This is an open access article under the terms of the Creative Commons Attribution License, which permits use, distribution and reproduction in any medium, provided the original work is properly cited.

1. Introduction

1.1. Importance of Detailed Paleobathymetry Grids for Southern Ocean Research

The Southern Ocean is a key player in the atmospheric and oceanographic fabric of the Earth. It developed from a series of isolated basins to a single circum-Antarctic ocean system with deep-water connections

between the Pacific, Atlantic, and Indian oceans in the Cenozoic. Especially since the Eocene-Oligocene Boundary at 34 Ma, the Southern Ocean has acted as one of the main controlling, but also sensitive, factors of the Earth's climate system. Fundamental issues, such as the massive and rapid growth of the Antarctic Ice Sheet at the Eocene-Oligocene Boundary as a result of declining atmospheric CO₂ (e.g., DeConto & Pollard, 2003) and/or the effect of thermal isolation of Antarctica (e.g., Kennett, 1977), are still strongly debated (Anagnostou et al., 2016; Scher et al., 2015).

Changes in atmospheric CO₂ levels have long been credited with the evolution of the Cenozoic climate (Pagani et al., 2005; Pearson et al., 2009) and the development of the Antarctic Ice Sheets. The current changes in the polar regions with dramatic ice loss (Rignot et al., 2008) and incursions of relatively warm Circumpolar Deep Water (CDW) onto the continental shelves (Dutrieux et al., 2014; Pritchard et al., 2012) call for studies of past polar environments in times of similar climatic and atmospheric conditions. Analogies for the modern potential collapse of the Antarctic Ice Sheets revealing tipping points and cascading effects of Southern Ocean warming include, for example, the Mid-Miocene Climatic Optimum and the warm period of the Pliocene.

Paleo-ice sheet models strongly depend on the subglacial bed topography and morphology, which have changed due to tectonic motion, for example, along the West Antarctic Rift System and glacial erosion, especially in large subglacial basins such as Wilkes Land or West Antarctica (Paxman et al., 2018; Wilson et al., 2012). A quantification of offshore sediment volume and potential source regions enhances paleotopographic reconstructions on a continental scale (Colleoni, De Santis, Siddoway, et al., 2018; Paxman et al., 2019).

Ocean currents in the Southern Ocean have also been strongly influenced by the changing bathymetry throughout the Cenozoic. The Southern Ocean widened significantly, for example, by almost doubling in size for the Australian-Antarctic Basin, since the onset of glaciation (Cande & Stock, 2004), allowing for more ocean current transport throughout the Southern Ocean.

Our current understanding of the paleocryosphere and paleo-ocean circulation hinges on our knowledge of the sedimentation patterns offshore Antarctica. They archive local and regional glacial sediment transport mechanisms (e.g., Close, 2010; Donda et al., 2008, 2020; Gohl, 2012; Hochmuth & Gohl, 2019; Huang & Jokat, 2016; Kim et al., 2018; Kuvaas et al., 2005) and bottom-water activities that can be related to glacial conditions (e.g., Huang et al., 2017; Rebesco et al., 1996; Uenzelmann-Neben, 2006; Uenzelmann-Neben & Gohl, 2012). The quantity of glacially derived sedimentation between different glacial outlets through time allows investigation of regional to local trends and developments, including issues to be addressed such as the following:

1. How much sediment has been eroded from the continent?
2. How active is the sediment transport at outlet glaciers in specific regions?
3. How does the transport and deposition of sediment change through time around Antarctica and into the Southern Ocean?

The structure of the seafloor sediments provides key information to investigate the behavior of the cryosphere and the oceans under different climate conditions. Since the establishment of the continental ice sheet around the Eocene-Oligocene Boundary, sediments deposited offshore Antarctica have recorded multiple stages of glaciation, ranging from ice sheets expanded onto the continental shelf, to the development of mountain/valley glaciers, and on to almost ice-free conditions (Passchier et al., 2019). Whereas extended ice sheets lead to high sedimentation rates along the continental shelf break and the slope, periods of reduced ice sheets are likely to have refilled sedimentary basins on the continent or continental shelves with only limited sedimentation across the continental shelves. During glacial periods, deeply cut glacial troughs can allow for the intrusion of bottom-water onto the shelf, triggering melting of the ice sheet from below. The conjugate margins are not directly influenced by ice masses, but the reorganization and variations in vigor of the ocean currents shape sedimentation patterns along the margins (e.g., Horn & Uenzelmann-Neben, 2015; Sauermilch, Whittaker, et al., 2019; Uenzelmann-Neben & Huhn, 2009).

Previously published global and regional paleobathymetric models oversimplify (Baatsen et al., 2016) or entirely omit the sedimentary column (Brown et al., 2006; Hayes et al., 2009). Recent inventories of the present-day sedimentary cover of the Southern Ocean reveal previous large underestimations of its sediment thickness (Lindeque, Gohl, Wobbe, et al., 2016; Straume et al., 2019; Whittaker, Goncharov, et al., 2013),

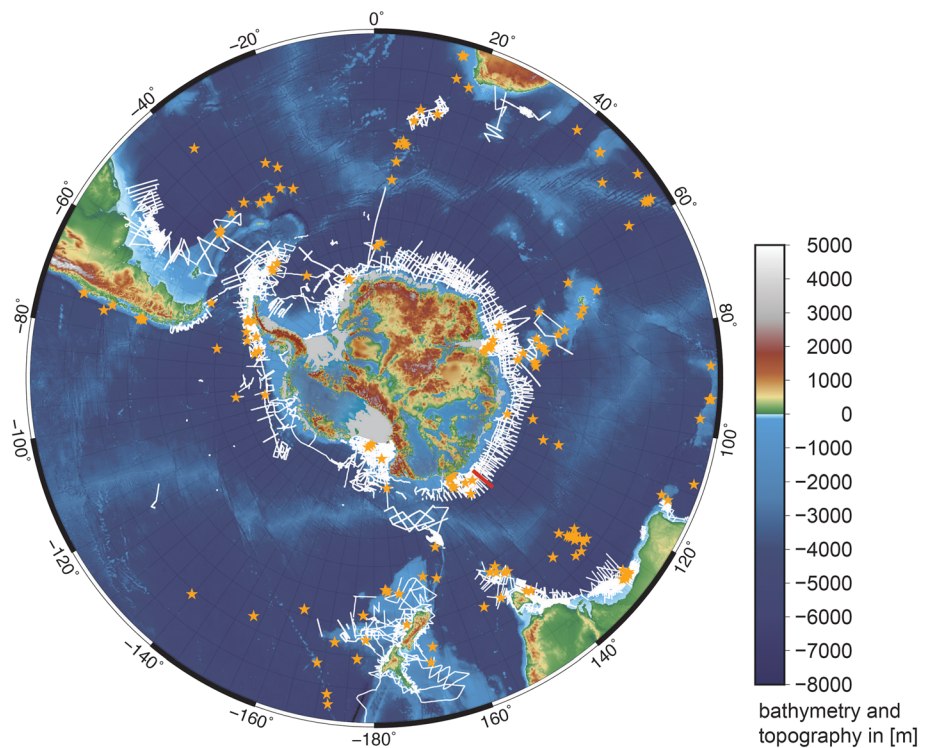


Figure 1. Bathymetric map of the Southern Ocean (Weatherall et al., 2015) with Antarctic subglacial topography after BEDMAP2 (Fretwell et al., 2013). White lines show seismic reflection profiles used in this study; orange stars indicate locations of IODP, ODP, and DSDP drill sites; and the red line marks an example seismic profile across the East Antarctic margin shown in Figure 3. Gray areas are modern ice shelves.

which makes a reevaluation of the sedimentary patterns and dynamics of deposition necessary. Recent paleoceanographic models that include improved paleobathymetries (e.g., Baatsen et al., 2018; Huang et al., 2017) report a high sensitivity of ocean current development and overall intensity to the changes in the seafloor geometry. A realistic representation of the seafloor morphology including seafloor roughness, seamounts, and shape of mid-ocean ridges according to spreading speed is crucial to produce more realistic paleo-ocean circulation models, which show, for example, eddy formation and therefore realistic heat transport (e.g., LaCasce et al., 2019; Viebahn et al., 2016).

Over the last decades, the regional network of seismic reflection profiles has improved significantly and the seismic stratigraphies of the Southern Ocean have been refined using multiple drilling efforts undertaken by the International Ocean Discovery Program (IODP) and its predecessor programs (Figure 1). Those efforts along the Antarctic, and conjugate, continental margins have facilitated the reinterpretation of the seismic data and calculation of paleobathymetric grids.

In this paper, we present a suite of new paleobathymetric grids of the Southern Ocean. We include a detailed description of our methodological approach (Figure 2) and the sources of potential errors invoked during the calculation and processing of paleobathymetric grids, which is critical for the use of the grids within the wider geoscientific community. We also present an interpretation and discussion of the patterns of sedimentation through time focusing on the mechanisms within the entire Southern Ocean. Further in-depth analyses of specific aspects of the sedimentary patterns in the Southern Ocean are provided in accompanying publications (Hochmuth & Gohl, 2019; Paxman et al., 2019; Sauermilch, Whittaker, et al., 2019).

2. Material and Methods: Unlocking the Bathymetry of the Past

2.1. Database and Seismic Stratigraphy

To undertake an assessment of the sediment distribution, create a unified stratigraphic correlation, and calculate sedimentary volumes in the Southern Ocean, we reexamined all available seismic reflection data from

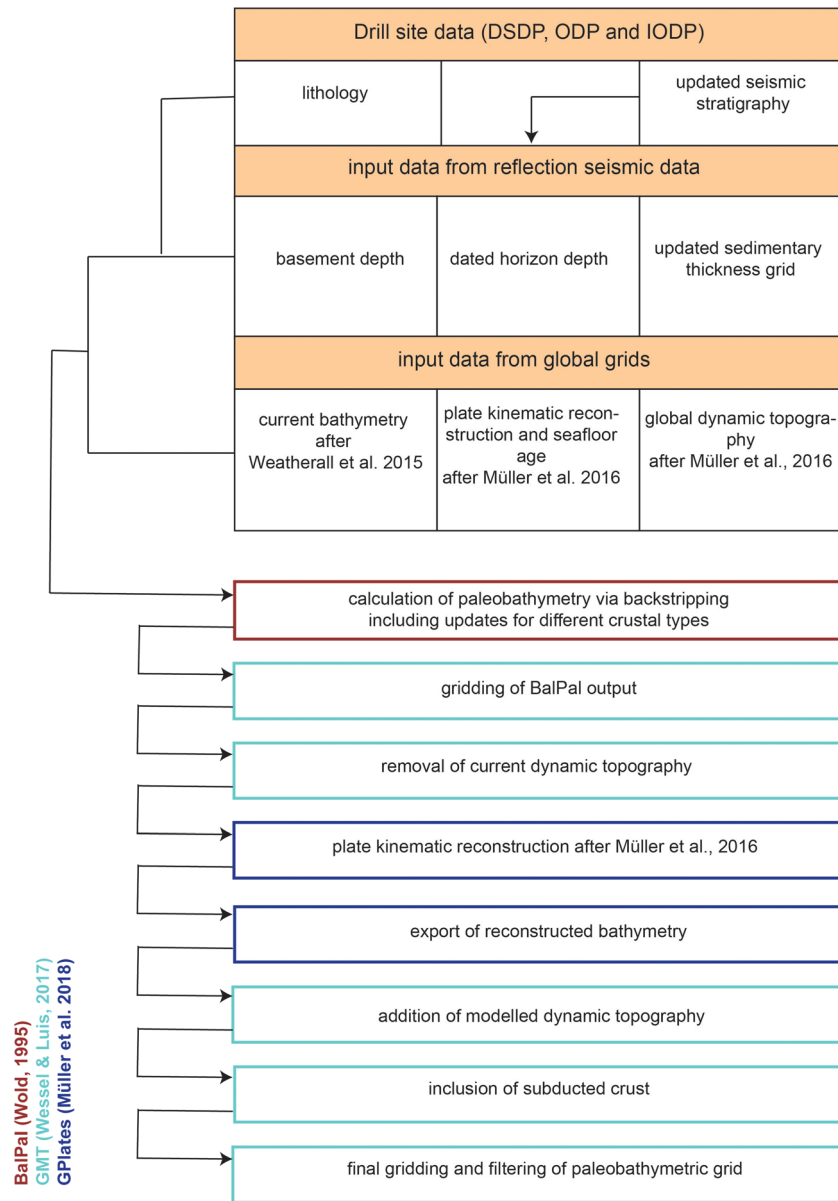


Figure 2. Workflow for deriving paleobathymetric grids, the colored boxes indicate software used for the step.

the Antarctic margins, their conjugate margins of South Africa, Australia, New Zealand, and South America, and the oceanic plateaus of the Southern Ocean (Figure 1). This includes data from 40 years of Southern Ocean seismic surveys by 13 nations from more than 150 individual research expeditions amounting to approximately 500,000 km of seismic reflection data. Data from the Antarctic margins were taken from the Antarctic Seismic Data Library System (SDLS) of the Scientific Committee for Antarctic Research (<https://sdls.ogs.trieste.it>; Figure 3). Data from the conjugate margins have been collected by the Alfred Wegener Institute or acquired from cooperation partners such as GNS Science for New Zealand and Geoscience Australia for the Australian margin. Vast areas of the Southern Ocean are not covered by seismic data (Figure 1), in particular the deep-sea areas far offshore (>1,000 km from the continental shelf edge). However, a thick sedimentary cover and significantly changing sedimentation rates are not expected in these areas as indicated by sparse single channel seismic profiles and the roughness of the seafloor which is visible from satellite-derived bathymetric data (Weatherall et al., 2015) (Figure 1) and represent the fabric of the oceanic crystalline basement. Some areas of the Antarctic margins are also poorly surveyed, which can lead to an overestimation or underestimation of the sedimentary volume of up to 20% in these areas. Whereas the

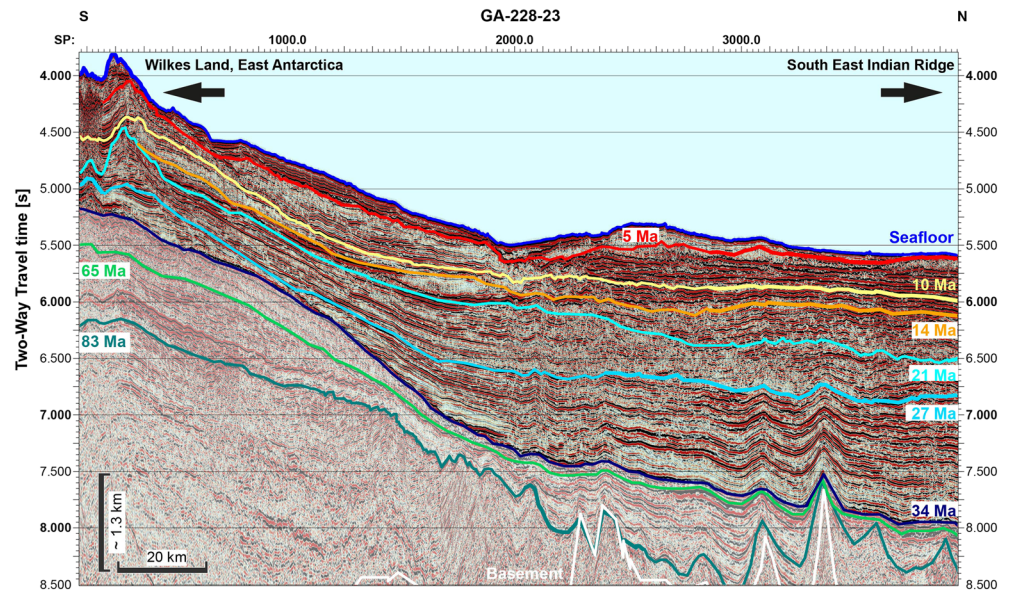


Figure 3. Example of a seismic section (GA-228-23) offshore Wilkes Land, East Antarctica, with identified and dated seismic horizons marked. The age of the horizons presented has been correlated to IODP 318 Site U1356. Location in Figure 1 (red line). Pre-rift (Basement to 83 Ma), rift sedimentation (83–65 Ma), and basement reflectors after Sauermilch, Whittaker, et al. (2019). Shaded areas display strata of pre-34 Ma age.

continental slope, rise, and adjacent deep sea offshore East Antarctica have been systematically mapped by Russian and Australian expeditions (Figure 1) (e.g., Close et al., 2007; Leitchenkov et al., 2007; Solli et al., 2007), most of the West Antarctic rise and deep sea are represented by much lower seismic line coverages (e.g., Gohl, Denk, et al., 2013; Kim et al., 2018; Larter et al., 2002; Lindeque, Gohl, Henrys, et al., 2016; Nitsche et al., 2000; Scheuer et al., 2006; Uenzelmann-Neben & Gohl, 2012, 2014) (Figure 1). The Antarctic continental shelf regions are also mapped in a variety of spatial coverage, which range from excellent coverage in the Ross Sea (e.g., Bart, 2003; De Santis et al., 1999) and Prydz Bay (e.g., Powell & Cooper, 2002) to medium coverage in the Amundsen Sea Embayment (Gohl, Uenzelmann-Neben, et al., 2013; Hochmuth & Gohl, 2013; Lowe & Anderson, 2002) and to very few lines without many crosslines in the Weddell Sea (e.g., Huang et al., 2014), the Totten glacier region (e.g., Gulick et al., 2017), and the Riiser Larsen Sea (e.g., Leitchenkov et al., 2008). Most of these coverage gaps are due to the remoteness of the region or the inaccessibility due to severe ice conditions even in the austral summer. Since our database includes seismic lines acquired over almost four decades (from the early 1980s to 2016), overall data quality, acquisition parameters (source volume/frequency, streamer length, shot frequency, etc.), and data processing (applied filters, velocity correction, multiple removal, etc.) and therefore the horizontal and vertical resolution of the data vary greatly and had to be considered for correlation between the different surveys of the same region. To achieve a “best fit” between different surveys, we used crosslines to verify reflector appearance and depth. The seafloor reflector has been checked against the bathymetry grid to verify representation of the water column.

To compute detailed paleobathymetries (Figure 2), we require (1) age constraints from drillcore data and (2) a unified correlation of various seismic stratigraphy for the entire Southern Ocean.

Since the beginning of scientific ocean drilling, borehole samples and data have been collected by the Deep Sea Drilling Project (DSDP), Ocean Drilling Program (ODP), Integrated Ocean Drilling Program, and International Ocean Discovery Program (both IODP) throughout the Southern Ocean (Figure 4). Today, data from almost 150 scientific drill sites in the Southern Ocean are publicly available. Downhole-logging and velocity check shots, which would give the smallest error margin for core-log seismic integration (Sauermilch, Mateo, et al., 2019), are only available for a small fraction of these drill sites. Therefore, most correlations rely on data acquired along the core. Especially deeper downhole, these values might invoke errors, due to poor recovery during the coring process and discontinuous core sections. The chronostratigraphic core data and associated seismic core-log integration data allow us to correlate and trace dated seismic horizons of layers, formation boundaries, and unconformities over large distances. On most conjugate

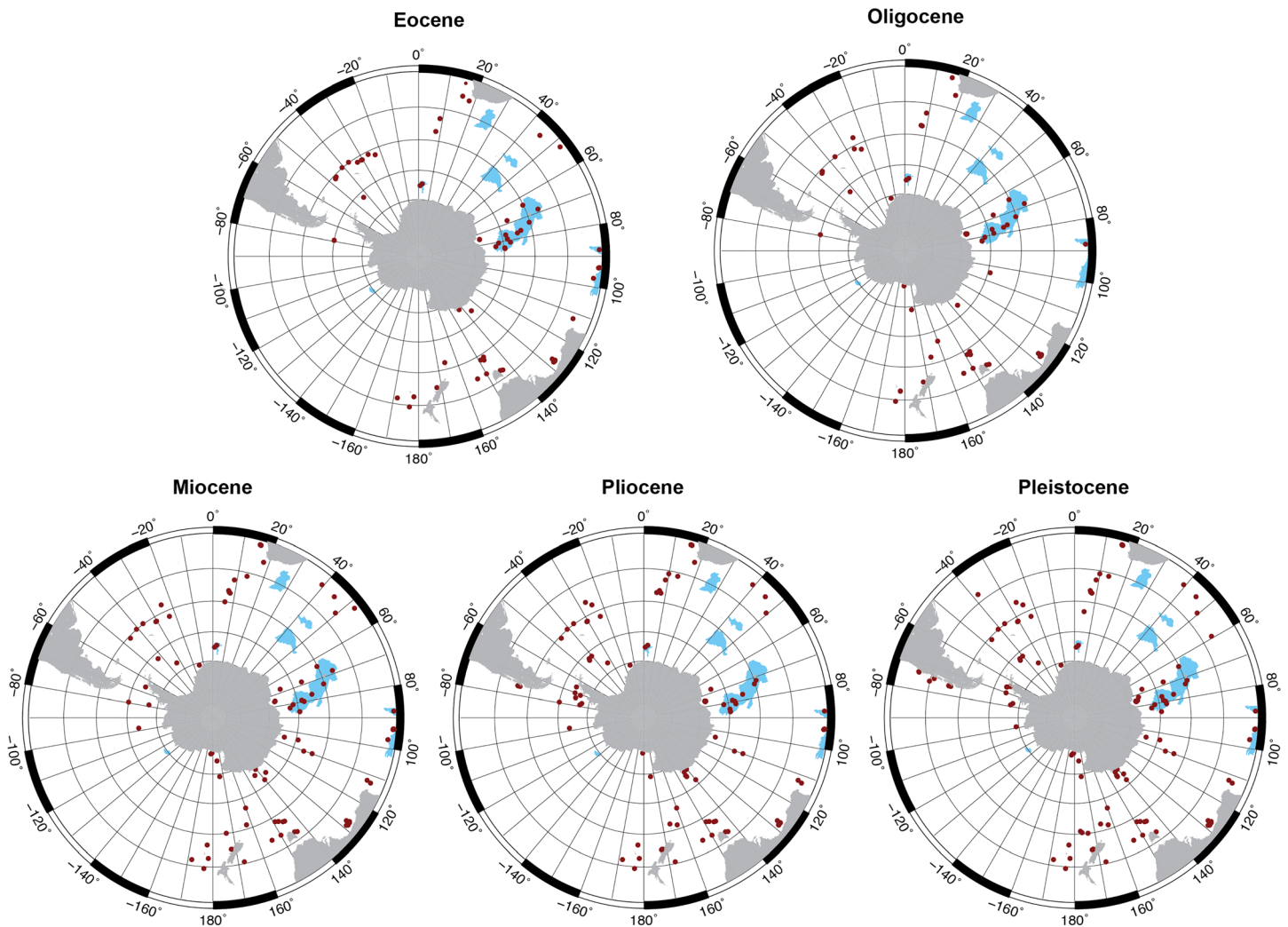


Figure 4. Present-day locations of IODP/ODP/DSDP drill sites in the Southern Ocean according to geological epochs from which sediments were cored and dated. Physical properties measurements on the core for depth conversion are available. Light blue areas show oceanic Large Igneous Provinces (LIPs).

margins, the seismic stratigraphy is significantly better constrained due to the availability of exploration wells (e.g., Sauermilch, Whittaker, et al., 2019; Totterdell et al., 2000). To properly correlate drill core data to seismic reflection data, we calculated synthetic seismograms at key sites (e.g., Wilkes Land margin Exp. 318 Site U1356 and Prydz Bay Exp. 188 Site 1165) using either downhole logging data sets or P wave velocity and density measurements of the cores, and then reevaluated the correlations made in the recent literature for the West Antarctic margin and the Weddell Sea (Uenzelmann-Neben & Gohl, 2012; e.g., Huang et al., 2014). By calculating the acoustic impedance and convoluting the outcome with a Ricker wavelet representing the seismic source used during data acquisition, we correlate the core data to seismic horizons. Based on this link, age information, lithology, and physical properties can be related to seismic horizons. Due to the sparseness of drill sites (Figures 1 and 4) this correlation is not always possible and would invoke large error margins. Therefore, we also need to rely on the interpretation of reflection characteristics and their related geological age (Table 1).

We started the compilation of our seismic stratigraphy for the entire Southern Ocean with published regional stratigraphies and then updated these regional models with more recently acquired drill site or seismic data that, for instance, provide more crosslines and reduced line spacing (Table 1). We identified two key horizons that can be traced throughout most of the Southern Ocean: a horizon representing the Eocene-Oligocene Boundary at 34 Ma and a horizon representing the middle Miocene at 14 Ma

Table 1
Overview of Previously Published Regional Seismic Stratigraphies of the Southern Ocean

Area	Reflector name	Reflector kind	Reflector age	Publication
Cosmonaut Sea, Cooperation Sea, Davis Sea	CS4	High amplitude continuous reflector	Earliest Oligocene 34 Ma	Leitchenkov et al. (2007)
Cosmonaut Sea, Cooperation Sea, Davis Sea	CS5	High amplitude continuous reflector	Early Miocene	Leitchenkov et al. (2007)
Wilkes Land	WL-U3	Regressive surface	~34 Ma (early Oligocene) hiatus 47.9–33.6 Ma	De Santis et al. (2003); Donda et al. (2003); Escutia et al. (2005, 2010)
Wilkes Land	WL-U4	Regressive surface	Late Oligocene	De Santis et al. (2003); Donda et al. (2003); Escutia et al. (2005, 2010)
Wilkes Land	WL-U5	Regressive surface wet-based ice influence on the rise sedimentation	Early Miocene 6 myr hiatus (23.12–17.5 Ma)	De Santis et al. (2003); Donda et al. (2003); Escutia et al. (2005, 2010)
Wilkes Land	WL-U5b	Regressive surface base of levee	Middle Miocene	De Santis et al. (2003); Donda et al. (2003); Escutia et al. (2005, 2010)
Wilkes Land	WL-U6	Regressive surface	Middle Miocene	De Santis et al. (2003); Donda et al. (2003); Escutia et al. (2005, 2010)
Wilkes Land	WL-U7	Regressive surface: transition to polar regime	Late Miocene	De Santis et al. (2003); Donda et al. (2003); Escutia et al. (2005, 2010)
Wilkes Land	WL-U8	Regressive surface Polar regime	Early Pliocene	De Santis et al. (2003); Donda et al. (2003); Escutia et al. (2005, 2010)
Eastern Ross Sea	RSU6	Continuous reflector that onlaps on structural highs, end of deposition of the RSS1	>26 Ma 30 Ma (early Oligocene)	De Santis et al. (1999)
Eastern Ross Sea	RSU5	Major erosional surface	21 Ma lower Miocene	De Santis et al. (1999)
Eastern Ross Sea	RSU4A	Low angle truncation surface with no clear evidence of large erosional features	19 Ma (19.23–17.5–16 Ma) Miocene age unclear	De Santis et al. (1999)
Eastern Ross Sea	RSU4	Erosional surface	14.1 Ma Miocene	De Santis et al. (1999)
Eastern Ross Sea	RSU3	First unconformity with a subhorizontal to gently landward-dipping sea-floor profile (after backstripping), erosional surface with an irregular relief	13.8–3.7 Ma late Miocene	De Santis et al. (1999)
Eastern Ross Sea	RSU2	Erosional surface	4 Ma Pliocene	De Santis et al. (1999)
Eastern Ross Sea	RSU1	Erosional surface	0.65 Ma Pleistocene	De Santis et al. (1999)
Amundsen Sea Embayment	ASS-u2	Unconformity	Early Miocene 21–19 Ma	Gohl, Uenzelmann-Neben, et al. (2013)
Amundsen Sea Embayment	ASS-u3	Unconformity	Middle Miocene 16–15 Ma	Gohl, Uenzelmann-Neben, et al. (2013)
Amundsen Sea Embayment	ASS-u4	Unconformity	Middle to late Miocene 14–9 Ma	Gohl, Uenzelmann-Neben, et al. (2013)
Amundsen Sea Embayment	ASS-u5	Unconformity	Pliocene 4–3 Ma	Gohl, Uenzelmann-Neben, et al. (2013)
Amundsen Sea	Green	Strong reflector	21–15 Ma early Miocene	Uenzelmann-Neben and Gohl (2012, 2014)
Amundsen Sea	Blue	Strong reflector	15–4 Ma middle to late Miocene	Uenzelmann-Neben and Gohl (2012, 2014)
Amundsen Sea	Orange	Strong reflector	4–0 Ma Pliocene to Pleistocene	Uenzelmann-Neben and Gohl (2012, 2014)
Ross Sea-Amundsen Sea Transect	AS-u3	Continuous strong reflector	~34 Ma, ~21 Ma, ~30 Ma	Lindeque, Gohl, Henrys, et al. (2016)

Table 1
Continued

Area	Reflector name	Reflector kind	Reflector age	Publication
Ross Sea-Amundsen Sea Transect	AS-u4	Continuous strong reflector	~26 Ma, ~18 Ma, ~25 Ma	Lindeque, Gohl, Henrys, et al. (2016)
Ross Sea-Amundsen Sea Transect	AS-u5	Continuous strong reflector	~20 Ma, ~14 Ma, ~21 Ma	Lindeque, Gohl, Henrys, et al. (2016)
Ross Sea-Amundsen Sea Transect	AS-u6	Continuous strong reflector	~15 Ma, ~9 Ma, ~15 Ma	Lindeque, Gohl, Henrys, et al. (2016)
Ross Sea-Amundsen Sea Transect	AS-u7	Continuous strong reflector	~9 Ma, ~6 Ma, ~12 Ma	Lindeque, Gohl, Henrys, et al. (2016)
Ross Sea-Amundsen Sea Transect	AS-u8	Continuous strong reflector	~4 Ma, ~5 Ma, ~8 Ma	Lindeque, Gohl, Henrys, et al. (2016)
Ross Sea-Amundsen Sea Transect	AS-u9	Continuous strong reflector	~2 Ma, ~2 Ma, ~1 Ma	Lindeque, Gohl, Henrys, et al. (2016)
James Ross Basin, Weddell Sea Antarctic Peninsula margin	Basement reflector	Reflector between chaotic and laminated reflections	Late Eocene to late Oligocene regional onlap surface within S5 is dated 32–37 Ma (late Eocene)	Smith and Anderson (2010)
James Ross Basin, Weddell Sea Antarctic Peninsula margin	Bottom of S4	Onlap surface	Latest middle early late Miocene	Smith and Anderson (2010)
James Ross Basin, Weddell Sea Antarctic Peninsula margin	Bounding surface to S3	Highly reflective regionally extensive unconformity, which truncates the topset beds of the underlying unit	Late Miocene	Smith and Anderson (2010)
James Ross Basin, Weddell Sea Antarctic Peninsula margin	Bounding surface to S2	Highly reflective regionally extensive unconformity, which truncates the topset beds of the underlying unit	Early to late Pliocene	Smith and Anderson (2010)
James Ross Basin, Weddell Sea Antarctic Peninsula margin	Bounding surface of S1	Unconformity change in stratigraphic architecture from progradational to aggradational strata	Latest Pliocene/Pleistocene to present	Smith and Anderson (2010)
Southeastern Weddell Sea	WS-u5	Prominent reflector unconformity	13 Ma late middle Miocene	Huang and Jokat (2016)
Southeastern Weddell Sea	WS-u6	Unconformity	7 Ma upper Miocene-lower Pliocene boundary	Huang and Jokat (2016)
Southeastern Weddell Sea	WS-u7	Unconformity	3 Ma lower Pliocene to upper Pliocene boundary	Huang and Jokat (2016)
Riiser-Larsen Sea	RLS-4	Unconformity	Middle Miocene or Oligocene	Solli et al. (2007)
Riiser-Larsen Sea	RLS-5	Highly reflective seismic surface, which onlaps the underlying RLS-4 at the base of the continental slope		Solli et al. (2007)
Riiser-Larsen Sea	RLS-6	Unconformity dipping gently or almost flat	Middle Miocene 15–11.6 Ma	Solli et al. (2007)
Great Australian Bight	Base Wobbegong Supersequence; U2	Unconformity	Paleocene (65–58 Ma)	Totterdell et al. (2000); Sauermilch, Whittaker, et al. (2019)
Great Australian Bight	Base Dugong Supersequence; U3	Strong reflector	Middle Eocene (~48 Ma)	Totterdell et al. (2000); Sauermilch, Whittaker, et al. (2019)
Bremer Subbasin	Base Eucla 1 Supersequence; U2	Unconformity	Paleocene (65–58 Ma)	Bradshaw (2005); Sauermilch, Whittaker, et al. (2019)
Bremer Subbasin	Base Eucla 2 Supersequence; U3	Strong reflector	Early Eocene (~50 Ma)	Bradshaw (2005); Sauermilch, Whittaker, et al. (2019)
Otway/Sorrell basins	Base Wangerrip Supersequence; U2	Strong reflector	Paleocene (~58 Ma)	Stacey et al. (2013); Sauermilch, Whittaker, et al. (2019)

Table 1
Continued

Area	Reflector name	Reflector kind	Reflector age	Publication
Otway/Sorrell basins	Base Nirranda Supersequence; U3	Strong reflector	Middle Eocene (~45 Ma)	Stacey et al. (2013); Sauermilch, Whittaker, et al. (2019)
Zealandia	Reflector R4	Erosional surface	Marshall-Para-unconformity 33–19.5 Ma	Horn and Uenzelmann-Neben (2015)
Zealandia	Reflector R5	Erosional surface	10.5–5 Ma	Horn and Uenzelmann-Neben (2015)
Zealandia	Reflector R2a		1.7 Ma	Horn and Uenzelmann-Neben (2015)
South Africa	LO		Early Oligocene	Uenzelmann-Neben and Huhn (2009)
South Africa	MM		Middle Miocene	Uenzelmann-Neben and Huhn (2009)
South Africa	LP		Late Miocene/early Pliocene	Uenzelmann-Neben and Huhn (2009)

(Figure 3). Other horizons can be traced within individual regions of the Southern Ocean (example from Wilkes Land margin in Figure 3), or represent slightly different times. Overall, we identified more than 50 regional horizons (Table 1) that have been proposed previously in the literature, which were used to tune our paleobathymetric reconstructions. In areas which are well dated and show thick glacial deposits, such as the Prydz Bay, Ross Sea, and Wilkes Land margin regions, we can rely on more detailed stratigraphies. Horizons in areas where drill core information is lacking and even long-distance seismic correlation is impossible (e.g., Riiser-Larsen Sea), we assessed and compared seismic reflection characteristics and sediment patterns with better constrained areas and then interpolated and extrapolated age models, accepting a large degree of uncertainty (± 3 Ma).

2.2. Selection of Time Slices for Paleobathymetric Reconstruction

In the following, we present nine different time slices of paleobathymetric reconstructions: 34, 27, 24, 21, 14, 10.5, 5, 2.6, and 0.65 Ma. These specific time slices were chosen because (1) they represent important developments and fundamental changes in the Southern Ocean and on a global scale (Figure 5) and (2) the age of these reflectors has been verified by drilling missions at multiple locations in the Southern Ocean (Figure 4). Target times for paleo-climate and ocean modeling are also included. We tried to identify time slices which enable us to make assumptions about the development of the Southern Ocean and its sedimentation patterns for the entirety of the last 34 Ma, focusing on major development in the cryosphere (e.g., first continental wide ice sheet [34 Ma] and potential collapse of marine parts of the ice sheet [14 Ma]), clearly established tectonic opening of ocean gateways (e.g., Tasmanian Gateway [27 Ma]) as well as massive increase in sedimentation rates at the continental shelf edges and their related northward growth on the Antarctic continent (e.g., late Miocene [10.5 Ma] and Pliocene/Pleistocene transition [2.6 Ma]). Specific time slices in between the presented slices can be calculated assuming constant sedimentation rates. If additional sediment thickness estimations and better age constraints on the strata will become available in the future, they can be integrated into the existing suite of grids and help recalibrate later iterations of the paleobathymetric grids. Users can adjust the presented grids to fit their specific purpose such as reconstructing different plate kinematic settings or adjust for a preferred dynamic topography model by using GIS software packages. The paleobathymetric reconstructions correspond to the paleotopographic reconstructions by Paxman et al. (2019) for 34 and 14 Ma. Given the error-margins within both reconstructions their 23 Ma reconstruction is compatible with the reconstruction of 24 Ma presented here. A joined suite of grids is currently in preparation and will be made available online (www.pangaea.de).

2.3. Crustal Parameters and Plate Tectonic Reconstruction

The thermal subsidence of the lithosphere plays a significant role in the calculation of paleobathymetry (Wold, 1995). We distinguish between four major categories of the Southern Ocean crust: continental crust, stretched continental crust, normal oceanic crust, and overthickened oceanic crust, such as seamount

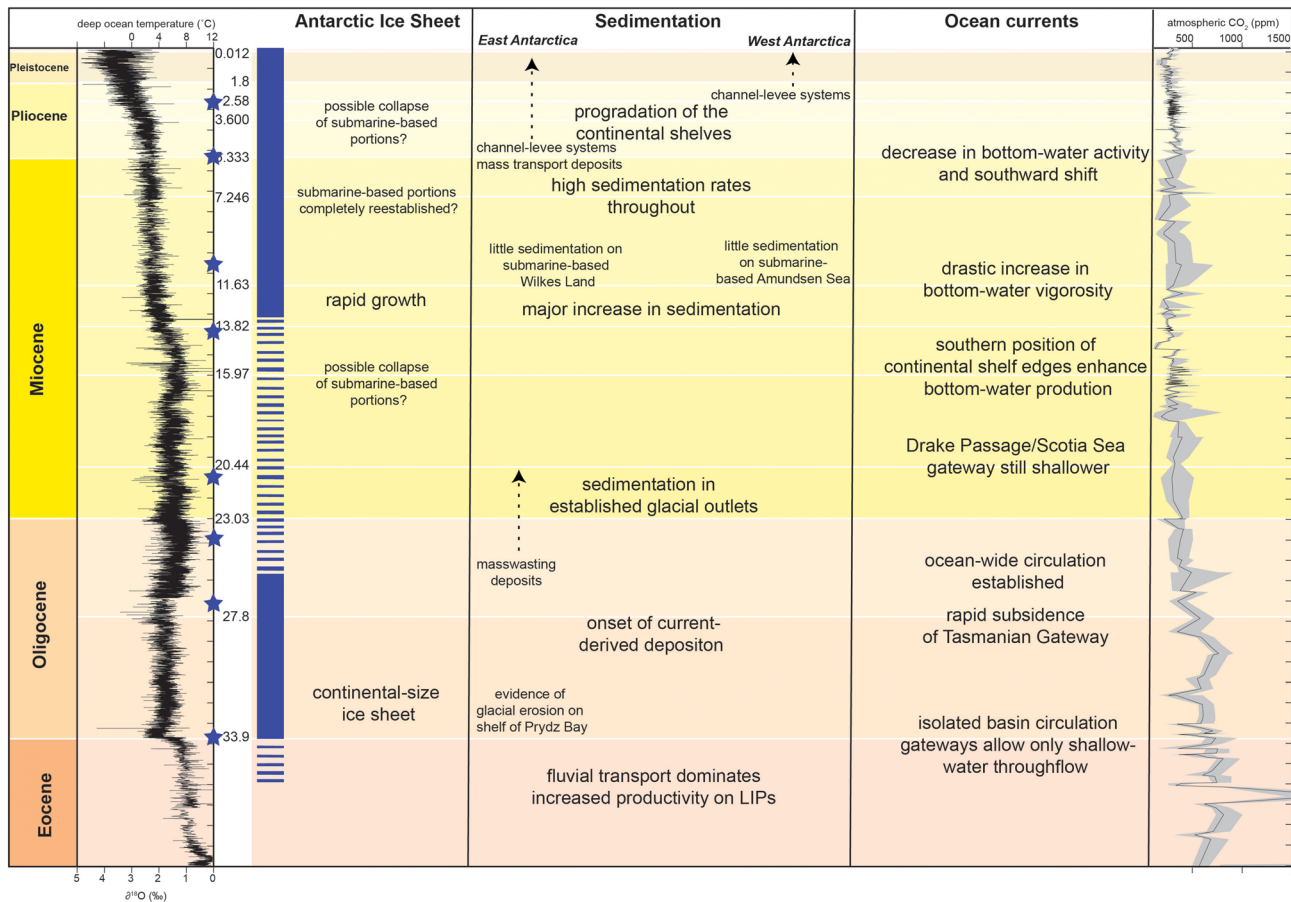


Figure 5. Overview of the development of the Antarctic Ice Sheets, sedimentation, and ocean current systems in the Southern Ocean since 34 Ma. $\delta^{18}\text{O}$ values and deep-sea temperature are after Cramer et al. (2009), atmospheric CO₂ after Foster et al. (2017), gray area indicates the potential error bar of the measurement. Blue stars mark ages of paleobathymetric grids of Figure 10.

provinces and Large Igneous Provinces (LIPs) (Figure 6) following Castelino et al. (2016). Normal continental crust has been parametrized after White et al. (1992). Areas of continental crust include continental areas as well as continental shelf areas, which were not subject to active extension and rifting during the reconstruction period. Stretched continental crust experienced extension during the reconstruction timeframe. An example is the South Tasman Rise, where crustal stretching due to the separation between Australia and Antarctica is still largely present during the Oligocene. We used a stretching factor (β) of 1.5 in accordance which is used for stretched continental crust between 30 and 15 km of crustal thickness (McKenzie, 1978). Stretched continental crust, normal oceanic crust, and overthickened oceanic crust have been further categorized based on extension/emplacement age and crustal thickness (Figure 6). We used the age-depth relationship in a plate-cooling model, the global depth and heat flow model by Stein and Stein (1992), which assumes a square-root function for the thermal subsidence of oceanic lithosphere younger than 20 Ma and an exponential function for older oceanic crust. This simple model reconstructs the target timeframe from 34 Ma to recent times reliably and significant changes in the reconstruction by using more sophisticated models (Richards et al., 2018) are not to be expected. The subsidence of stretched continental crust also follows an exponential trend in relationship to its stretching factor β (McKenzie, 1978).

Oceanic plateaus differ from surrounding ocean crust by their thickness (ranging from 10 to more than 30 km) and their emplacement age (Table 2). Most volcanic oceanic plateaus of the Southern Ocean formed in the Cretaceous and are, therefore, relatively unchanged throughout the Cenozoic. Smaller volcanic edifices, such as the Marie Byrd Seamounts, evolved during the early Cenozoic (Kipf et al., 2014), changing local subsidence patterns and creating bathymetric highs. Volcanic edifices that emplaced since the

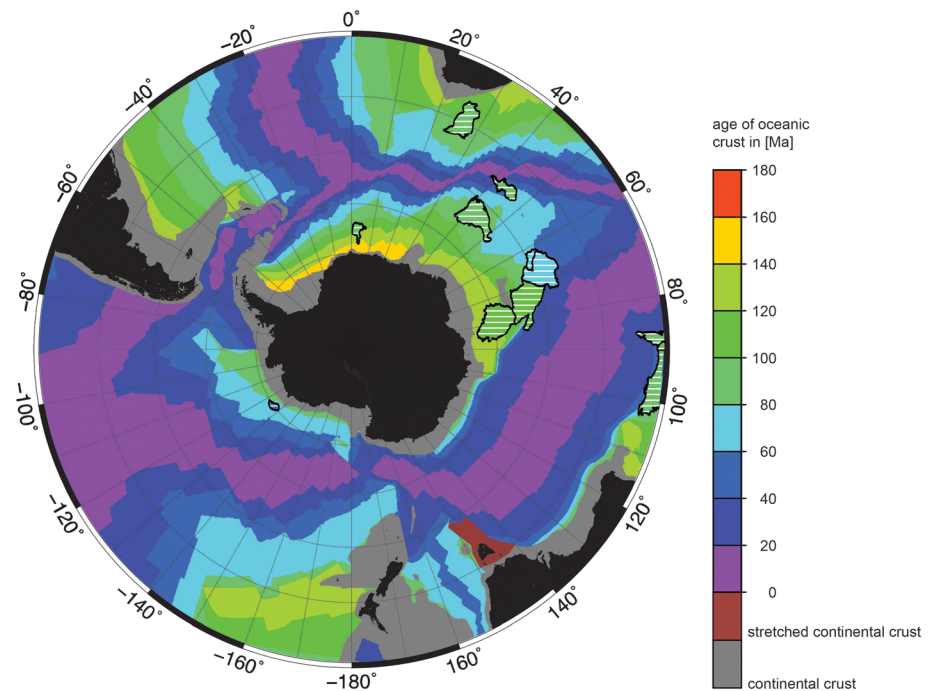


Figure 6. Overview of crustal categories and ages (after Müller et al., 2016) used for the paleobathymetric reconstruction. Hashed areas indicate overthickened oceanic crust (Table 2). Black areas indicate present-day coastlines. Note: the color bar is chosen as discreet for better visualization, whereas the true values of the oceanic crust have been used for the reconstruction.

Eocene-Oligocene Boundary have been replaced with normal ocean crust prior to their emplacement and included with corrected thickness after emplacement. If no additional data for the crustal set-up is available, volcanic structures mimic their modern appearance after their emplacement.

The Cenozoic Southern Ocean developed after the initial breakup of Gondwana, separating the East Antarctic continent and the continental blocks of West Antarctica from the continents of Africa, India, Australia, Zealandia, and South America, starting in the late Jurassic (Seton et al., 2012, and references therein; Müller et al., 2016). Although most oceanic spreading centers were well established by 34 Ma, it is important to note that subduction had not yet ceased along the Pacific margin of the Antarctic Peninsula at 34 Ma.

The opening of the ocean gateways, namely, the Tasmanian Gateway and the Drake Passage/Scotia Sea Gateway, is regarded as being finalized by the early Oligocene (Bijl et al., 2013; Scher et al., 2015), although

Table 2

Additional Parameters Used for the Reconstruction of Overthickened Crust, Such as Large Igneous Provinces, in the Southern Ocean (Locations in Figure 4)

Area	Emplacement age, reactivation age (Ma)	Crustal thickness (km)	References
Agulhas Plateau	100	25	Gohl and Uenzelmann-Neben (2001), Parsiegla et al. (2008)
Broken Ridge	100, 90	18	Francis and Raitt (1967), Charvis and Operto (1999)
Conrad Rise	90	16	Francis and Raitt (1967)
Crozet Plateau	90	16	Recq et al. (1998)
De Cano	90	22	Recq et al. (1998)
Kerguelen Plateau (North)	70	21	Charvis and Operto (1999)
Kerguelen Plateau (Central)	88	17	Charvis and Operto (1999)
Kerguelen Plateau (South)	120	23	Gohl et al. (2007)
Marie Byrd Seamount Province	65, 54	13	Kipf et al. (2014)
Maud Rise	100, 75	25	Jokat et al. (2004), Parsiegla et al. (2008)
Meteor Rise	100, 65	25	Raymond et al. (1991)
Transkei Basin	100	22	Gohl et al. (2011)

the exact timing and dimension of the deep-water openings is still a matter of debate (Barker & Thomas, 2004). Since the early Cenozoic ocean crust of the Drake Passage was subducted at the Scotia Arc, we base our paleobathymetric reconstructions of this area on the model by Eagles and Jokat (2014).

We use the most recent global plate reconstruction model by Müller et al. (2016) to implement the tectonic parameters for our paleobathymetric grids. In comparison with an earlier paleobathymetric model of the Southern Ocean (Hayes et al., 2009), this newer plate reconstruction model accounts, for example, for a lower spreading rate between East Antarctica and Australia (Cande & Stock, 2004), which narrows the Antarctic-Australian Basin for the Oligocene, as well as for slower spreading between Zealandia and the conjugate crustal blocks of West Antarctica (Wobbe et al., 2012) as well as the aforementioned reconstruction of the Drake Passage and Scotia Sea (Eagles & Jokat, 2014). All these recent improvements to the plate-kinematic reconstruction result in different positions of the continents compared to older reconstructions. We therefore encourage a rigorous crosschecking of plate reconstruction by using multiple different paleogrids.

We applied the GPlates software (Müller et al., 2018) to reconstruct the grid nodes to their paleoposition and used a paleomagnetic reference frame including global apparent polar wander, since this aligns best for using the bathymetry in a modeling context to couple oceanic and atmospheric processes (Baatsen et al., 2018; van Hinsbergen et al., 2015). By comparing a hotspot-reference frame with the used paleomagnetic reference frame, paleolatitudes in the Southern Ocean vary up to 10° depending its location and distance to the pole. Before using the presented paleobathymetric grids, comparability to other input files as well as the suitability of the reference frame for the scientific question needs to be ensured and if necessary adjusted.

2.4. Calculation of Sediment Volumes

Seismic data are collected in seconds of two-way travel time. The conversion from recorded seismic two-way travel time in seconds (Figure 3) to depth in meters is an essential step for developing a geological model. Most of the seismic data available for this study have been recorded with multichannel streamer systems, but the *P* wave velocity-depth data used for data processing are rarely available. In these cases, we used available velocity-depth models as sample sections to compare and interpolate the velocities associated with strata of different depth (Huang et al., 2014; Lindeque, Gohl, Wobbe, et al., 2016; Uenzelmann-Neben & Gohl, 2012). In the Australian-Antarctic sector, sonobuoy data were used for a potentially more accurate *P* wave velocity-depth conversion of the sedimentary column (see Sauermilch, Whittaker, et al., 2019, for details). From the collected velocity data, we produced regional velocity grids, and used them to convert horizon data from time to depth domain. This conversion was also verified using drill records and core-log integration results from the DSDP, ODP, and IODP drill sites (Figure 4). Time-depth relationships can vary significantly (up to 55%) depending on the drilled material and type of measurement (Sauermilch, Mateo, & Boaga, 2019), although the error in mainly siliciclastic environments, such as most of the Antarctic continental margin environments, is comparatively small (~10%) to ensure a more reliable conversion.

For areas lacking seismic reflection data coverage, we interpolated and extrapolated “synthetic” horizons based on the following basic assumptions: (1) deep-sea strata terminate against the oceanic basement where there is an interpreted magnetic lineation of the corresponding age, (2) strata terminate against basement highs, (3) strata crop out at the seafloor on the Antarctic continental shelves (Stagg, 1985; e.g., Gohl, Uenzelmann-Neben, et al., 2013) if not otherwise indicated (e.g., Weddell Sea; Jokat & Herter, 2016), and (4) local information of the stratigraphic set-up of conjugate margins are extrapolated regionally (e.g., South Africa). Point (3) is constrained in the few areas of Antarctic margin where seismic data exist which show oceanward dipping sedimentary sequences that were truncated by advances of grounded ice in glacial times. The outer shelves are often characterized by progradational sequences with deposits of glacially transported sediments across the shelf edge. We integrated the recent assessment of circum-Antarctic shelf progradation and shelf growth through time by Hochmuth and Gohl (2019) as an important paleobathymetric feature.

After time-depth conversion of the seismic horizons, we calculated the observed thickness (Figures 7 and 8) and volume of the sediment units (Table 3) as well as sedimentation rates (Figure 9). Sedimentation volumes for the sediment basins were calculated with the Generic Mapping Tool (GMT) routine *grdvolume*.

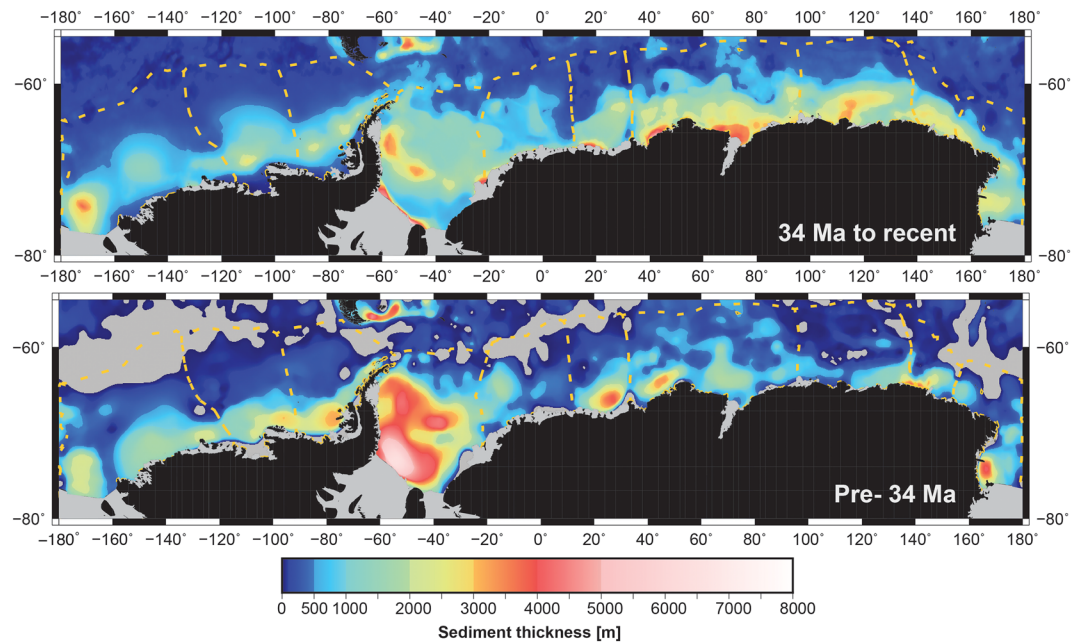


Figure 7. Circum-Antarctic sediment thicknesses before the development of a continent-wide ice sheet (pre-34 Ma) and after (34 Ma to recent). Yellow dashed lines are different sectors of the Southern Ocean (see Table 3 for sediment volumes). Gray areas indicate areas with no data coverage and post-34 Ma oceanic crust. Black areas indicate present-day coastlines.

To compare observed volume estimations, we separate the sediment grid into different source sectors (yellow lines in Figure 7), which have also been used by Paxman et al. (2019). The sectors along the Antarctic margin take basement morphology (e.g., Gunnerus Ridge and Central High in the Ross Sea), prevailing ice sheet flow and downslope and along-slope sediment transport mechanisms into account. This approach assumes that the source areas on a sector-wide scale have not changed since the Eocene-Oligocene Boundary. Comparing our result with previous observed volumes of the post-Eocene sediment volumes by Wilson et al. (2012) (Table 3), we see that observed sediment volumes in the Prydz Bay and Wilkes Land sectors of East Antarctica were significantly underestimated in comparison to previous overall estimates used for paleotopographic reconstruction (Wilson et al., 2012). Our calculations result in two to five times the maximum observed volume estimated by Wilson et al. (2012) for Prydz Bay and the Wilkes Land margin, respectively. Sediment volumes of the Dronning Maud Land margin as well as the George V margin were moderately underestimated previously (see Table 3). An important factor in this development is clearly the additional seismic data acquisition along the margins to better constrain the sedimentary cover. The Amundsen Sea sector is the only sector for which we obtained a smaller sediment volume compared to Wilson et al. (2012).

2.5. Backstripping Method

There are numerous publications where paleobathymetries are computed. Some methods calculate the paleobathymetry along seismic profiles, and interpolate between the profiles (Huang et al., 2014). Others do not consider, or oversimplify, the sedimentary column (Brown et al., 2006; Hayes et al., 2009) which is justified in deep-sea areas but causes large errors in many areas of the Southern Ocean, where the sediment thickness exceeds several kilometers (Lindeque, Gohl, Wobbe, et al., 2016; Straume et al., 2019; Whittaker, Goncharov, et al., 2013).

We used a modified version of the BalPal routine (Wold, 1995), which is equipped to deal with such large and diverse data sets (Figure 2) to unload, and decompact sediments on the seafloor. This methodology also isostatically compensates the seafloor using an Airy-style isostasy and accounts for eustatic sea-level change. It is important to note that there is no regional sea-level curve for the Southern Ocean available yet, therefore this reconstruction is based on global estimates, which might not represent the regional sea-level change

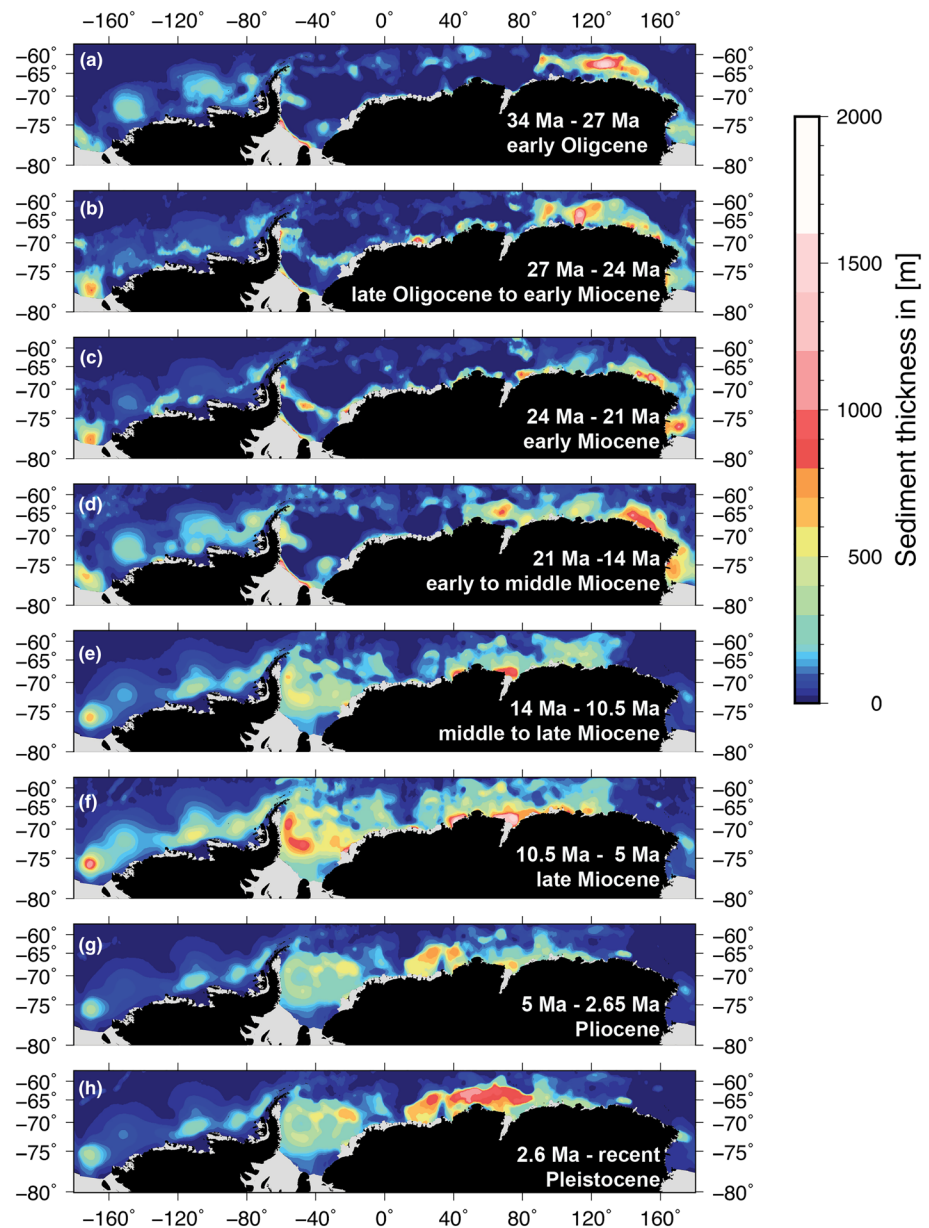


Figure 8. Total sediment deposited during the labeled interval. These grids reveal the changes in the distribution of main sediment deposition. Sedimentation has been assumed to occur at a constant rate between seismic reflectors. For reflectors and regions refer to Table 1. (a) 27 to 34 Ma; (b) 24 to 27 Ma; (c) 21 to 24 Ma; (d) 14 to 21 Ma; (e) 10.5 to 14 Ma; (f) 5 to 10.5 Ma; (g) 2.6 to 5 Ma; (h) recent to 2.6 Ma. Gray areas indicate areas with no data coverage and post-34 Ma oceanic crust. Black areas indicate present-day coastlines.

accurately. BalPal works entirely on a grid-cell basis. This allows the user to adjust the resolution of the resulting grid, but also integrate grids of higher resolutions in areas where they are available without the need to downsample to match other low-resolution grids. Every grid cell includes information about the underlying crust (lithology, age, thickness) (Figure 6 and Table 2) as well as information on the sedimentary column for every specific layer (age, lithology, depth, thickness) (Figure 8). The algorithm is equipped to interpolate between horizons and also allows for unconformities/nondeposition within the strata. Wold (1995) originally used the BalPal routine for a $1^\circ \times 1^\circ$ resolution paleobathymetric grid of the North Atlantic. The software has since been modified and used in ocean basins, including parts of the Southern Ocean (Castelino et al., 2016), with an increase in spatial resolution. We calculated the grids of this study at a spatial resolution of $0.1^\circ \times 0.1^\circ$.

Table 3
Overview of the Post-34 Ma Sediment Volume (in 10^6 km^3) of Antarctic Sectors in Comparison to Previous Volume Estimates (Wilson et al., 2012)

Study	Weddell Sea	Dronning Maud land margin	Riiser Larsen Sea	Prydz Bay	Wilkes Land margin	George V land coast	Western Ross Sea	Eastern Ross Sea and Marie Byrd Land	Amundsen Sea	Bellingshausen Sea	
											Min
Observed Volume in 10^6 km^3	Wilson et al. (2012)	2.40	0.54	0.63	1.17	0.54	0.48	1.50		1.60	1.00
		4.40	0.66	0.77	1.43	0.66	0.72	3.00		2.60	2.00
This study and Paxman et al. (2019)		3.04	0.82	0.9	3.63	3.28	1.08	1.26	1.73	1.27	1.42
Computed mass in 10^{15} t	Paxman et al. (2019)	3.88	0.57	0.49	3.25	3.48	1.15	2.53	2.14	1.09	1.35

Note. Shading shows a large (>100%) (orange) or moderate (>30%) (yellow) increase of the sediment volume in comparison with Wilson et al. (2012); green-shaded sector shows a reduction of sediment volume.

2.6. Finalizing Paleobathymetric Grids

Computed paleo-depths, generated with BalPal (Figure 2), were reconstructed to their paleo-positions using GPlates and the plate tectonic model of Müller et al. (2016). Reconstructed paleo-bathymetries were adjusted for long-wavelength mantle-driven dynamic topography using the preferred dynamic topography model from Müller et al. (2018) Model 1, since this model performs best over Cenozoic timeframes and especially allows a good representation of the topographic history of Gondwana cratons. In areas where oceanic crust has been subducted along the South American and western Antarctic Peninsula margins as well as along the South Sandwich Arc of the Scotia Sea, we filled these gaps (Supporting Information Figure S1) with picked depth points from previous reconstructions (Hayes et al., 2009) ensuring consistency with the plate kinematic environment. Since these areas have most likely not undergone major sedimentation given that they originate far away from major sediment sources, the subsidence of the oceanic crust as used by Hayes et al. (2009) is a valid approximation.

Finally, our paleobathymetric grids were carefully filtered to minimize effects caused by stitching of areas with different crustal parameters similar to Straume et al. (2019) as well as excessive unrealistic values (Figure 6) and edited to remove gridding artifacts. Continental regions above sea-level were masked. The morphology of the mid-ocean ridges was reconstructed according to their spreading rates at the given reconstructed time (Figure 6).

3. Uncertainty Assessment

Our reconstruction uses numerous large data sets, all with potential errors and uncertainties. Here we provide an assessment of these errors and uncertainties.

3.1. Sediment Stratigraphy and Isopachs

The accuracy of the horizon depths, their age, and the resulting sediment volumes strongly depend on the availability of seismic reflection data and how closely they can be tied to drill sites. In the absence of drill sites, horizons can be identified by their seismic character. A change in sedimentation style or a discordance are assigned ages from their geological context such as the onset of the ACC, which need to be adjusted in the future, if borehole data become available, or major reinterpretations of the geological context come to light. While tracing horizons along the continental rise and the deep sea is relatively straight forward even over long distances, shelf strata and sequences on the continental slope are often disturbed and subject to redeposition of older material. This can lead to an overestimation of sediment volume for younger times and an erroneous assumption of a later erosional date. Volume calculations inherit these uncertainties. We tried to address these uncertainties by carefully reexamining the available data sets, especially in areas where multiple data sets were integrated into a single grid through multiple cross lines and the integration of newly available data. Since a seismic horizon represents a geological event and not necessarily a constant age, the event age can gradually change along a horizon (e.g., Lindeque, Gohl, Henrys, et al., 2016), which will affect paleobathymetric reconstructions on a local and regional scale.

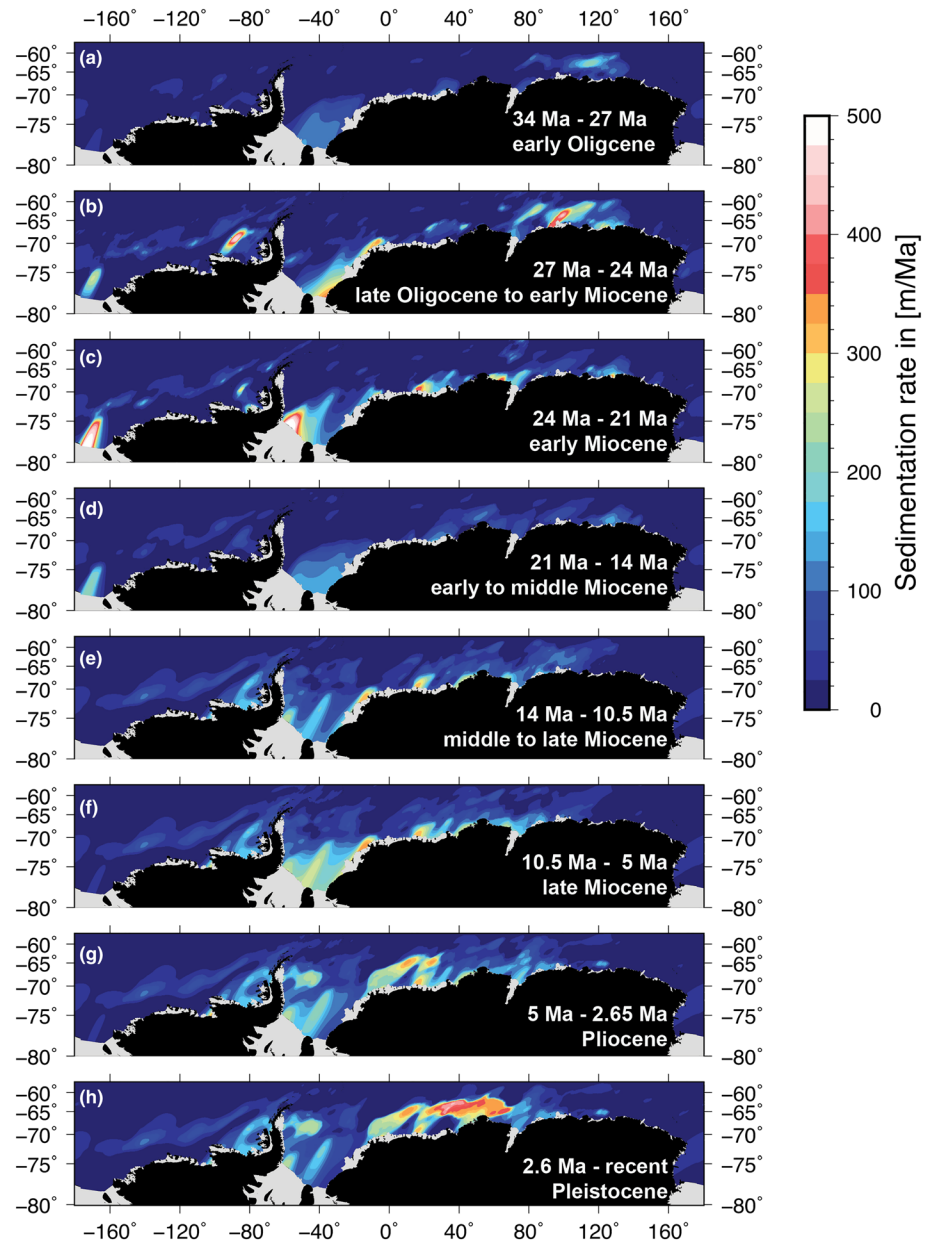


Figure 9. Sedimentation rates during intervals (a) 27 to 34 Ma; (b) 24 to 27 Ma; (c) 21 to 24 Ma; (d) 14 to 21 Ma; (e) 10.5 to 14 Ma; (f) 5 to 10.5 Ma; (g) 2.6 to 5 Ma; (h) recent to 2.6 Ma. Sedimentation has been assumed to occur at a constant rate between seismic reflectors. For reflectors and regions of occurrence refer to Table 1. Gray areas indicate areas with no data coverage and post-34 Ma oceanic crust. Black areas indicate present-day coastlines.

Another important uncertainty to consider is the erosion and redeposition of sediments by ocean currents and the ice sheet. Since there are no dedicated sediment provenance studies yet for the Southern Ocean that can reveal multiple stages of sediment deposition and erosion (e.g., on the continental shelf, subsequent erosion by an advancing ice sheet, deposition on the continental slope and later erosion by slope parallel currents or mass wasting events), the isopach maps only report about the most recent deposition. This causes potential overestimation of sediment volumes toward younger time slices and toward the deeper ocean.

3.2. Crustal Parameters and Subsidence

Since this study focusses on an ocean-wide reconstruction and a more accurate representation of the sediments in the paleobathymetric grids, some geodynamic effects were neglected. Although we accounted for

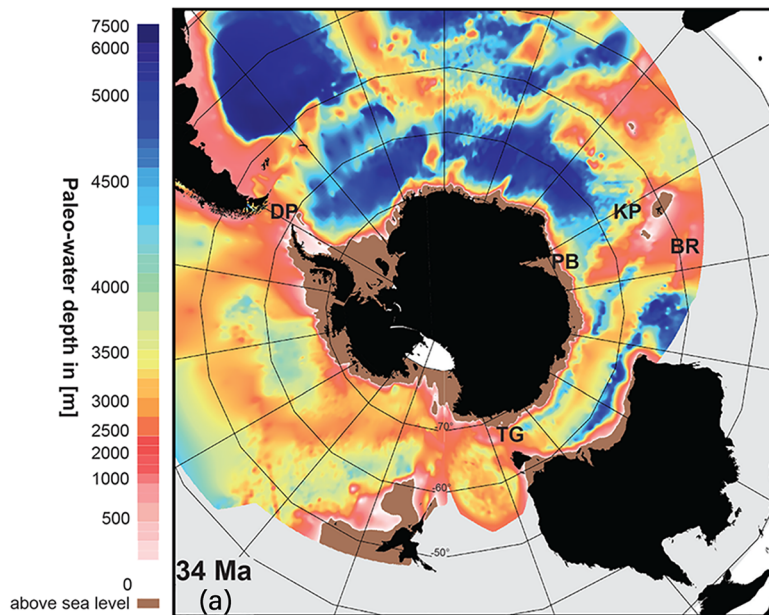


Figure 10. Paleobathymetry of the Southern Ocean: (a) 34 Ma representing the Eocene-Oligocene Boundary; (b) 27 Ma representing the early Oligocene; (c) 24 Ma representing the Oligocene/Miocene transition; (d) 21 Ma representing the earliest Miocene; (e) 14 Ma representing the middle Miocene; (f) 10.5 Ma representing the late Miocene; (g) 5 Ma representing the early Pliocene; (h) 2.6 Ma representing the Pliocene/Pleistocene Boundary; (i) 0.65 Ma representing the middle Pleistocene. Note that the color scale used is tailored to reveal changes in bathymetry especially in the crucial depth between 700 and 2,500 m and is therefore not continuous. Black areas indicate modern coastlines to facilitate orientation. Areas on the panel without grid coverage is shown in light gray. For interpolated areas of now subducted oceanic crust refer to Figure S1. Abbreviations: AS = Amundsen Sea; BEL = Bellingshausen Sea; BR = Broken Ridge; DP = Drake Passage; KP = Kerguelen Plateau; PB = Prydz Bay; RS = Ross Sea (RS); SAB = Sabrina Aurora Basin; TG = Tasmanian Gateway; TO = Totten Glacier; VA = Vanderford Glacier; WED = Weddell Sea; WLB = Wilkes Land Basin; WA = West Antarctica.

long-wavelength mantle-driven dynamic topography, we did not correct for regional uplift on the continent, such as the uplift of Marie Byrd Land dome in West Antarctica (Spiegel et al., 2016) or uplift related to volcanic activity along the West Antarctic Rift System (van Wyk de Vries et al., 2018), which mainly affects the continental shelf regions.

Volcanic edifices in the oceanic realm, such as LIPs and seamounts, are carefully included in the reconstruction, but the available crustal parameters could introduce uncertainties and bias into the models. We calculated subsidence of the LIPs and other volcanic features similar to oceanic crust but adjusted for their greater crustal thickness. This assumption may not be valid for all LIPs. For instance, a thermal model for the Ontong-Java Plateau (Ito & Clift, 1998) predicts a significantly faster subsidence than reconstructed from drill core data. The crustal thickness of most LIPs is derived from 2-D seismic refraction profiles (Table 2) assuming a block-like constant thickness across the plateaus. We treated the large Kerguelen Plateau as a system of multiple plateaus with different crustal thicknesses and emplacement/reactivation ages (Table 2). Seamounts were treated with subsidence rates similar to those for oceanic crust, but have been removed from the grid in times before their emplacement such as the Balleny Seamount chain (Finn et al., 2005).

An accurate plate kinematic reconstruction plays an important role in the paleobathymetric reconstruction of the Southern Ocean, in particular for the gateways of the Southern Ocean. By comparing recent global (Müller et al., 2016; Seton et al., 2012) and regional (Cande & Stock, 2004; Eagles & Jokat, 2014; Whittaker, Williams, et al., 2013; Wobbe et al., 2012) reconstructions, it becomes evident that some unresolved issues still exist for reconstructions of some areas, for instance, the different terranes of West Antarctica, the timing of cessation of subduction along the western Antarctic Peninsula, the formation of the Scotia Sea, and, therefore, the connection from the Pacific to the Atlantic plate circuit. The last major development within plate kinematic reconstructions of the Southern Ocean is the change in spreading rate along the Australian Antarctic ridge, which reduces the area of the Oligocene Australian-Antarctic basin (Cande & Stock, 2004; Whittaker et al., 2007), influencing the internal circulation of the basin and the

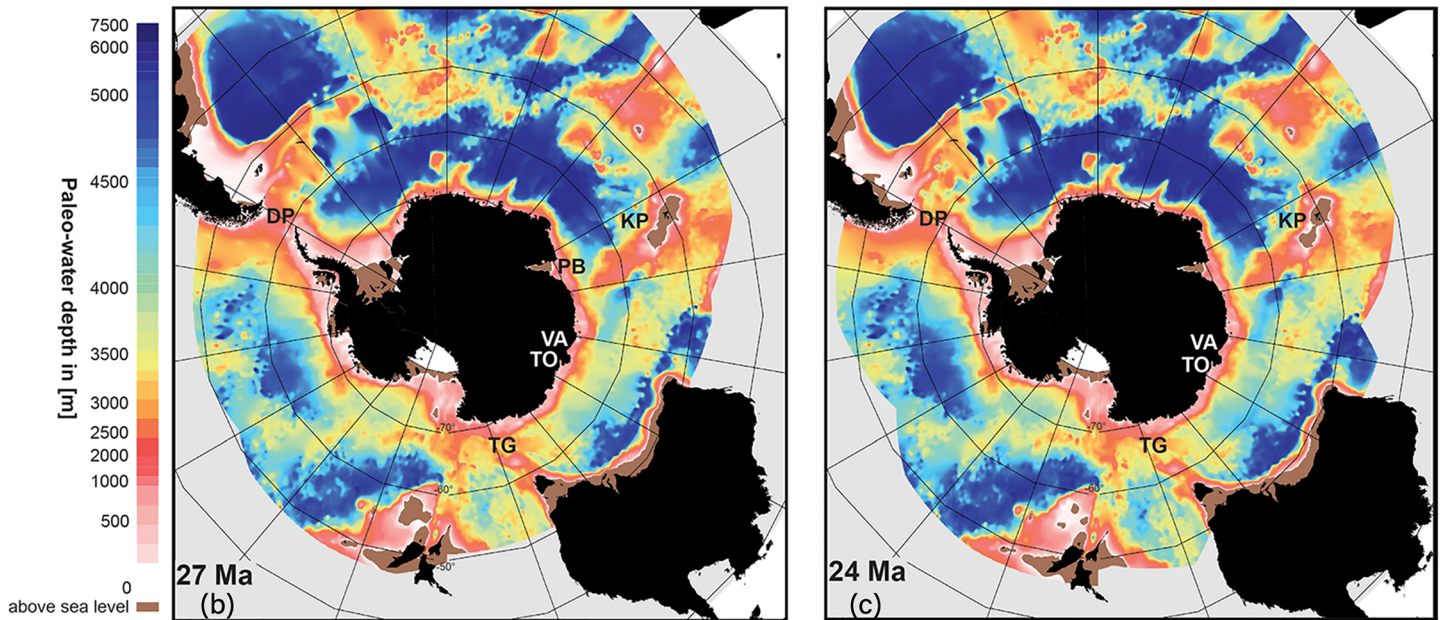


Figure 10. (continued)

development of the ACC, which is included in Müller et al. (2016), but is still significantly wider in older reconstructions still widely used in the community. Future improvements in plate kinematic models as well as dynamic topography models will improve future iterations of the paleobathymetric grids.

3.3. Paleobathymetries of the Antarctic Continental Shelves

The paleobathymetry of the Antarctic continental shelves is important for understanding the interplay between the ice sheet, the fringing ice shelves, and the ocean. Overall, glaciated shelves are much deeper than their conjugates on corresponding margins (Weatherall et al., 2015). If the continental shelves are deep enough, CDW can intrude onto the shelf through glacial trough and scour systems (e.g., Assmann et al., 2013; Nakayama et al., 2017; Schodlok et al., 2017). If these relatively warm waters reach cavities beneath ice shelves, it causes melting from below, destabilizing the ice shelves and grounding zones, and forcing retreat. When calculating paleobathymetries, the continental shelves pose additional difficulties. Even very good seismic data and drill core coverage, for example, in the Ross Sea, cannot constrain the volume of sediments which were deposited on the shelf during interglacial times and subsequently eroded during a following glacial advance. Without dedicated provenance studies of, for example, reworked microfossils deposited in younger strata, it is difficult to assess how much sediment has been redeposited on the continental shelf and slope by a repeatedly advancing ice sheet.

Due to the difficulties outlined above, our Antarctic shelf paleobathymetries are maximum depth estimates. The complete paleo-sediment volumes on the shelves prior to an expansion of the ice sheet and thus their paleodepths are likely shallower. A comparison of our shelf paleobathymetries with drill core-derived, or paleotopographical modeling, paleodepths indicate similar depth ranges. However, drill site coverage on the Antarctic continental shelves is sparse. The sites located in Prydz Bay and the Ross Sea are not representative of all Antarctic continental shelves. Nevertheless, at DSDP Site 270 in the Ross Sea, the transition from a paleosol horizon to a shallow marine environment at 25.9 Ma can be observed (Kulhanek et al., 2019; Leckie & Webb, 1983). The transition from subaerial to shallow marine also occurs in the paleobathymetric reconstruction, but occurs slightly earlier at 27 Ma, although this is well within the potential error margin of the calculations. Paleotopographic reconstructions show the same timeframe for flooding of the continental shelf at this locality (Paxman et al., 2019; Wilson et al., 2012). In Prydz Bay, the Eocene-Oligocene Boundary in ODP Holes 742A and 1166A show evidence of a shallow glacial coastal plain environment (e.g., Passchier et al., 2017), similar to Alaska-type piedmont glaciers. In our 34 and 27 Ma reconstructions, the Prydz Bay

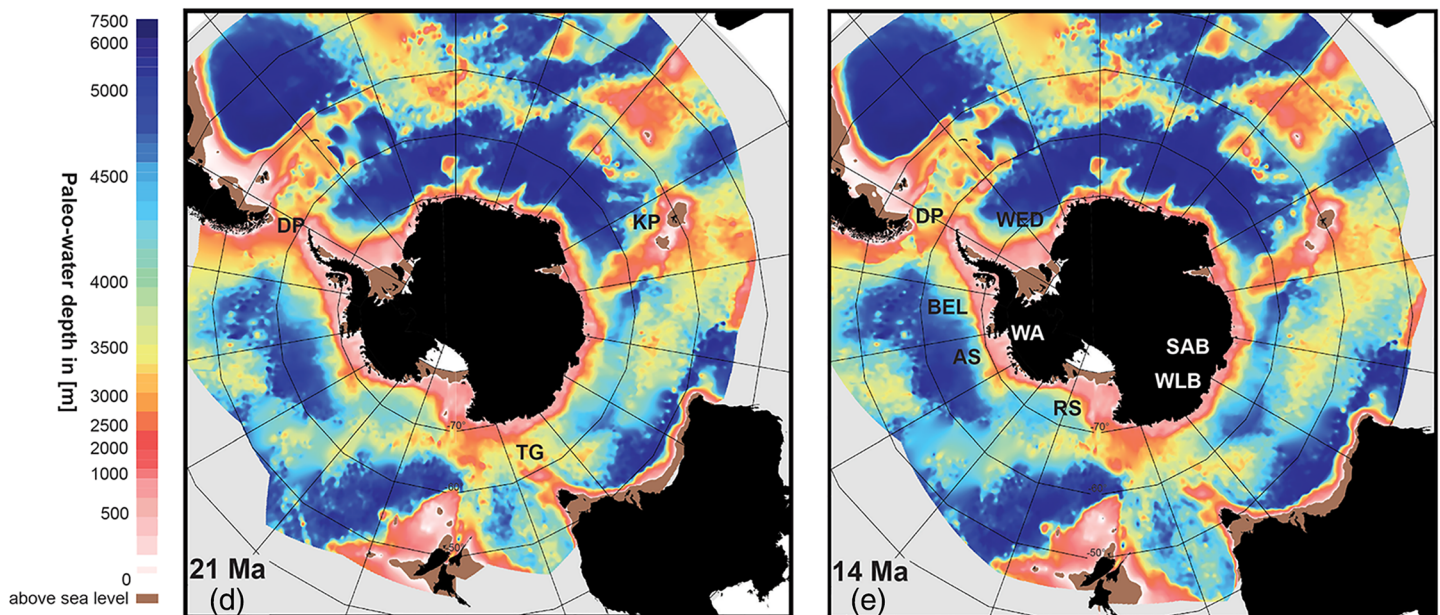


Figure 10. (continued)

region is subaerial at these times, which supports the presence of piedmont glaciers, originating along the flanks of the embayment.

4. Results and Discussion

We present and discuss the paleobathymetric grids of eight time slices from the Eocene-Oligocene Boundary to the Pleistocene (Figure 10), representing times of major paleoclimatic changes. We discuss ocean-wide trends in paleobathymetry and sediment fluxes with relationship to the cryosphere and the ocean circulation in the Southern Ocean (Figure 9).

4.1. Pre-Oligocene: Fluvial Influx and Sediment Drifts in Isolated Basins

Sedimentation in the Southern Ocean prior to the Oligocene (Figure 7) was dominated by vast fluvial deltas on the continental shelves and current-controlled sediment transport and deposition in the isolated basins that evolved after Gondwana breakup (Gohl, Uenzelmann-Neben, et al., 2013; Gulick et al., 2017; Sauermilch, Whittaker, et al., 2019). Most of the sedimentation took place in the basins of the continental shelves (Prydz Bay, Weddell Sea, Ross Sea, Amundsen Sea, Bellingshausen Sea, and Sabrina Coast) and in the deep sea leeward of basement highs (Gunnerus Ridge, Astrid Ridge) and LIPs (Figure 7). Numerous ocean-current systems, interpreted from analyses of contourite and drift deposits, differ greatly those of modern oceans (Castelino et al., 2016; Gruetzner & Uenzelmann-Neben, 2016; Horn & Uenzelmann-Neben, 2015; Sauermilch, Whittaker, et al., 2019; Uenzelmann-Neben & Huhn, 2009). While most LIPs in the Southern Ocean developed in the Cretaceous (Table 2), second- and later-stage volcanism led to large amounts of erosion and high bioproductivity on their shallow zones (Diekmann et al., 2004; Diester-Haass, 1995).

4.2. Oligocene: Gateway Opening and the First Continental-Wide Ice Sheet

The Southern Ocean in the Oligocene is dominated by the interplay of two main processes: the tectonically controlled widening and deepening of the oceanic gateways (Eagles & Jokat, 2014; e.g., Scher et al., 2015), and the potential continent-wide establishment of an Antarctic Ice Sheet (DeConto & Pollard, 2003; Galeotti et al., 2016; Pollard & DeConto, 2019). We developed three distinct bathymetric models for the Oligocene, a reconstruction at the Eocene-Oligocene Boundary representing the Oi-1 event (Figure 10a), a reconstruction representing the end of the early Oligocene at 27 Ma (Figure 10b), and a reconstruction of the transition between the Oligocene and the Miocene at 24 Ma (Figure 10c).

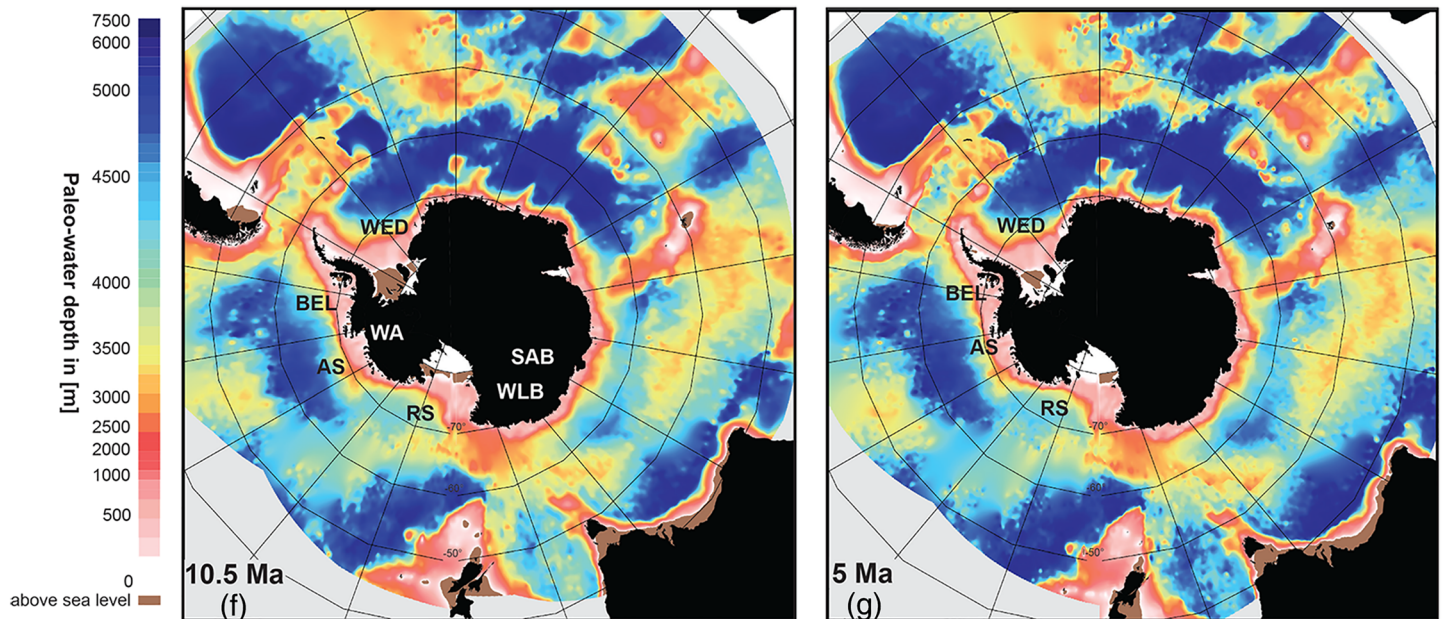


Figure 10. (continued)

The Eocene-Oligocene Boundary is marked by a sharp temperature decrease, interfered from $\delta^{18}\text{O}$ data (Cramer et al., 2009; Zachos et al., 2008) and an increase in atmospheric CO_2 (Foster et al., 2017; Zachos et al., 2008) (Figure 5). The actual size and stability of an early Antarctic Ice Sheet is still debated for this time slice (DeConto & Pollard, 2003; e.g., Carter et al., 2017; Galeotti et al., 2016), but a similar size to that of the recent Antarctic Ice Sheet can be assumed (e.g., Galeotti et al., 2016; Liu et al., 2009). The terrestrial area of Antarctica was approximately 25% larger than today (Paxman et al., 2019; Wilson et al., 2012). Oi-1 glaciation is described as an “over-shoot” within the $\delta^{18}\text{O}$ record (Figure 5) as a reaction to ice-sheet growth, which returned quickly to a relatively stable glacial environment in the early and middle Oligocene (Galeotti et al., 2016). The late Oligocene is marked by a temperature increase reaching late Eocene conditions. Atmospheric CO_2 drops in multiple steps within the Oligocene mark the change-over from a high to a low atmospheric CO_2 -world (Figure 5).

Based on drill records (Figure 4) and seismic reflection data, the Eocene-Oligocene Boundary is one of the better dated seismic horizons of the Southern Ocean. Additionally, the seismic characteristics of this horizon, separating glacially influenced sedimentation and from previous nonglacial sedimentation are clearly traceable in seismic data (Figure 3). The growth of an ice sheet caused an increase in ice rafted debris and strong bottom currents. One of the major questions connected to this time slice concerns the extent and volume of deep-water exchange through the oceanic gateways of the Tasmanian and Drake Passage/Scotia Sea gateways (Figures 10a–10c). Our paleobathymetry model indicates with a very small portion (<150 km) of the gateway below 1,000 m water depth the bathymetric conditions for only a shallow to medium water exchange at the Tasmanian gateway. This supports the findings of Scher et al. (2015), which point to an onset of deep-water exchange through the Tasmanian gateway at around 30 Ma (Figure 10a). Similar to Eagles and Jokat (2014), our model shows the bathymetric conditions for a shallow to medium water exchange through the Drake Passage/Scotia Sea gateway across an area of approximately 300 km. Furthermore, the Kerguelen Plateau and its conjugate Broken Ridge LIP are in parts subaerial and were separated by a narrow rift system (approximately 250 km at 2,800 m water depth), likely limiting and/or rerouting the water mass exchange from the Indian Ocean into the Antarctic-Australian Basin (Figure 10a). Sediment accumulation rates and patterns are similar to those in prevailing sedimentation of the Eocene (Figure 8a). High sedimentation rates proximal to LIPs are due to high bioproductivity as the result of an interplay between the strengthened polar frontal system and a high degree of preservation on a shallow oceanic plateau (Diekmann et al., 2004; Diester-Haass, 1995; Villa et al., 2014) (Figure 9a).

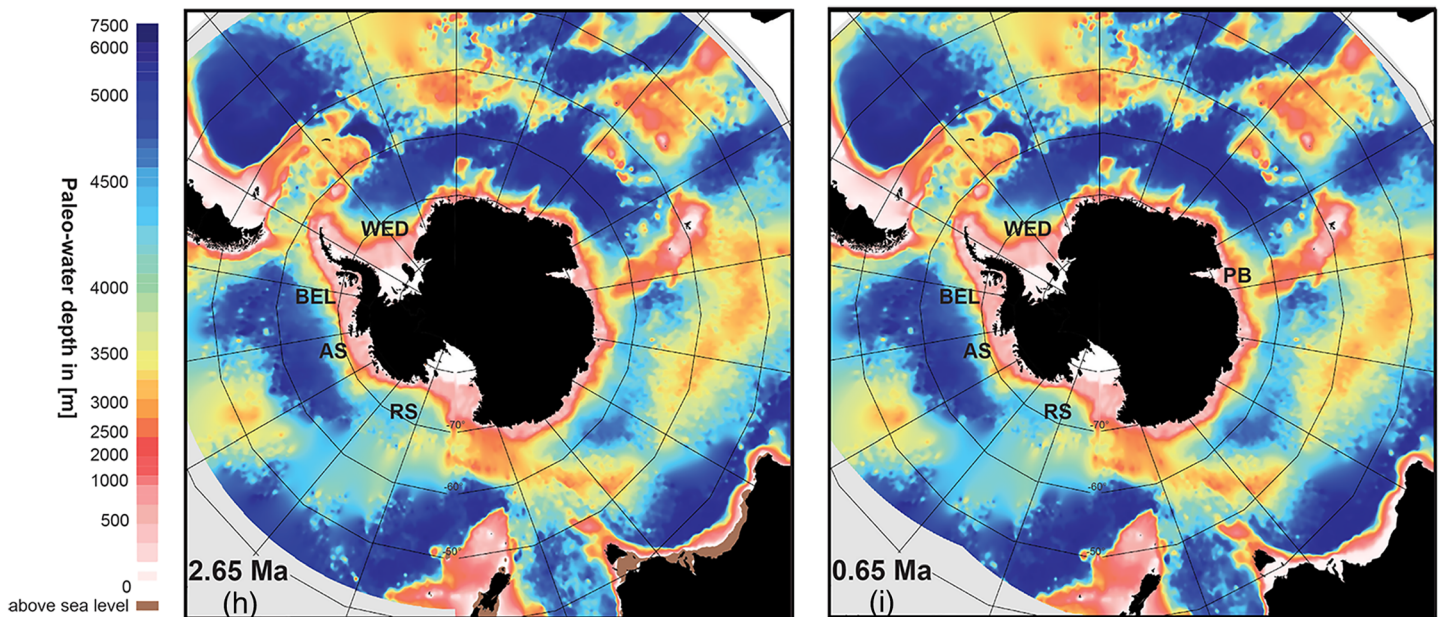


Figure 10. (continued)

Similar high sedimentation rates can also be observed in the isolated southern Australian sector of the Southern Ocean (Figures 8a and 9a).

Large gyre circulation was progressively dominated by the ACC during the early Oligocene after its establishment. The Southern Ocean gateways as well as the Pacific sector of the Southern Ocean deepen between 34 and 27 Ma, allowing easier through flow and exchange between the different ocean sectors (Figures 10a and 10b). The prevailing cold conditions caused the onset of bottom-current derived deposition along the continental rises. The first advance of an East Antarctic Ice Sheet onto the continental shelf of Prydz Bay can be seen in seismic reflection data by an erosional surface cutting through pre-Oligocene strata (Cooper & O'Brien, 1998; Kuvaas & Leitchenkov, 1992). The continental shelf of the Prydz Bay experiences flooding within the early Oligocene (Figures 10a and 10b). High sedimentation rates along the continental slope of much of East Antarctica point to strong onshore erosion by the ice sheet (Figures 8b and 9b). These sediments represent a major portion of the post-Eocene deposition within the Southern Ocean, especially offshore East Antarctica, marking a first major sedimentation surge. Prograding turbidite systems transport the sediments toward the foot of the continental slope (Close, 2010; Escutia et al., 2000). West Antarctica experienced an increasing sediment transport during the Oligocene (Figures 8a–8c and 9a–9c), but the deposition remained mainly in deltaic systems on the continental shelf.

Our work reveals that the glacial dynamics appear comparable to that of today since similar outlets with increased sedimentation on the continental slope and rise are observed, but the amount of sediment deposited offshore ice streams has varied dramatically through time. For instance, sedimentation offshore the Vanderford Glacier was much higher (~400 m/Ma) than offshore the Totten Glacier (~180 m/Ma) during the Oligocene, whereas in more recent time slices, the output by the Vanderford Glacier is clearly dwarfed by the Totten region (Figures 8b and 9b).

Sedimentation decreases along the entire Antarctic margin with the onset of the Late Oligocene Warm Period (Figures 8c and 10c), and mass wasting deposits became common along the East Antarctica margins (e.g., Donda et al., 2008).

4.3. Miocene: Foundation of Today's Ice-House World

The Miocene lays the foundation to today's icehouse world with a series of events which shape our understanding of the climate system and inform our predictions of rising CO₂ in the atmosphere (Figure 5). The mid-Miocene was characterized by a temperature increase of about 4 °C warmer than today. CO₂

estimates range from 280 to 500 ppm for the early and middle Miocene (Foster et al., 2017) (Figure 5). Ice sheet models predict the presence of an East Antarctic Ice Sheet, which retreated during interglacials in regions where the ice sheet was previously grounded below sea level (Gasson et al., 2016). The West Antarctic Ice Sheet was significantly smaller than today, and its submarine-based regions likely collapsed during severely warm interglacials (Gasson et al., 2016). Following this warm climatic interlude, the Mid-Miocene Climate Transition transferred the Antarctic and Southern Ocean toward prevailing cold climate conditions. With these paleoclimatic conditions in mind, we discuss three paleobathymetric grids: the early Miocene at 21 Ma (Figure 10d), the end of the Mid-Miocene Climatic Optimum at 14 Ma (Figure 10e), and the late Miocene at 10.5 Ma (Figure 10f).

Early Miocene sedimentation was driven by processes similar to those during the middle Oligocene, with established glacial outlets and little sedimentation in the Atlantic sector of East Antarctica (Figure 8d). Although a deep-water exchange through the Southern Ocean gateways was established, the Drake Passage/Scotia Sea gateway was shallower than in modern times (~2,000 m water depth compared to today's 3,800 m) (Figure 10d). Paleobathymetric reconstructions for 21 (Figure 10d) and 14 Ma (Figure 10e) show that continental shelf breaks were further south, closer to the coasts, than today, which is likely related to intensified gyre circulation (Huang et al., 2017) throughout the Southern Ocean.

The end of the Mid-Miocene Climatic Optimum and the following transition into colder climates increased sedimentation rates throughout the Southern Ocean by a growing, wet-based ice sheet (Figures 8e and 9e), leading to a second surge of sediment input into the Southern Ocean. Along the margins, limited sediments were supplied from submarine-based parts of the ice sheets such as the Wilkes Land Basin, Sabrina-Aurora Basin, and West Antarctica. A full glacially driven sedimentation was not established until the end of the Miocene (Figure 8f). Uenzelmann-Neben (2018) reported this phenomenon regionally by comparing the Bellingshausen and the Amundsen Seas. Major continental margin progradation was also observed in different sectors of the Antarctic margin between the late Miocene and early Pliocene (De Santis et al., 1999; Donda et al., 2020; Escutia et al., 2005; Hochmuth & Gohl, 2019). The different onset times of full glacial conditions point to a delay in the expansion of the ice sheets across the submarine-based parts of the ice sheets in both East and West Antarctica. This enables onshore sedimentation in continental subglacial basins to continue through the middle to late Miocene in these regions, and starve the adjacent offshore regions. Sedimentary strata of unknown age have been identified within the subglacial basins, based on inversion of magnetic and gravimetric data (Aitken et al., 2014).

The paleobathymetric reconstructions for 21 and 14 Ma with up to 600 m water depth show relatively deep continental shelves (Figures 10d and 10e). This could facilitate the incursion of warm CDW onto the shelf, the interpreted main cause for the retreat of submarine-based ice sheets. The paleobathymetry of the continental shelves is a maximum depth estimate and now eroded sediments could flatten the water depth by multiple decameters (see section 3.3). Recent paleotopographic reconstruction of the Antarctic continent implies a similar deep depth ranges for the continental shelves (Paxman et al., 2019). A more detailed assessment of the paleobathymetry of the shelves using local and regional backstripping methods (Colleoni, de Santis, Montoli, et al., 2018), which include better constrained lithological parameters from drill sites, is needed to fully understand the role of the Miocene continental shelves. The depth of the continental shelves is especially interesting for assessing the potential of ice sheet collapse during the Mid-Miocene Climatic Optimum as indicated by ice sheet models (e.g., Gasson et al., 2016). Throughout the late Miocene Southern Ocean, the increasing vigor of the ocean-bottom current system is well documented by the onset and intensification of sediment drift building processes (Cooper & O'Brien, 1998; Escutia et al., 2005; Kuvaas et al., 2005; Rebesco et al., 1996, 2002; Sangiorgi et al., 2018; Uenzelmann-Neben & Gohl, 2012). Since the end of the Miocene, the main glacial outlets dominate the sedimentation along the margin (Figures 8f and 9f), and most regions experienced progradational growth of the outer continental shelf (Bart, 2003; De Santis et al., 1999; Escutia et al., 2012; Hochmuth & Gohl, 2019; O'Brien et al., 2004).

4.4. Pliocene: Warm Intermezzo and Rapid Ice Sheet Retreat

Similar to the Mid-Miocene Climatic Optimum, the warm periods in the Pliocene are of major interest for paleoclimate modeling to simulate analogues of present and near-future climate changes. The Pliocene warm periods atmospheric CO₂ concentrations were slightly higher than today's, the global temperature was 2–3 °C warmer (Figure 5), but the global sea-level was about 25 m higher (e.g., Dumitru et al., 2019).

Based on ice sheet models, it has been proposed that high summer temperatures led to substantial meltwater production, causing hydrofracturing of ice shelves and a subsequent retreat of the submarine-based ice sheets of West and East Antarctica (DeConto & Pollard, 2016). The extent of this potential collapse of the marine parts of the ice sheets are still highly debated.

Guided by the availability of dated seismic reflectors, we calculated a paleobathymetric grid for 5 Ma (Figure 10g) and the transition between the Pliocene and the Pleistocene at 2.6 Ma (Figure 10h).

An overall decline in sedimentation rates can be observed along the Antarctic margins from the late Miocene to the Pliocene (Figure 8f). Although most deposition concentrated near outlets of large glacial catchment areas, the Indian Ocean sector received most of the glacially transported sediments (Figures 8f and 9f). It is important to note that age constraints on this margin are very limited and it is possible that these strata, at least in part, is of earlier, for example, Miocene origin. Shelf progradation moved the shelf edges further oceanward by up to 200 km, especially those at the embayments of West Antarctica, the Weddell Sea, and Ross Sea (Hochmuth & Gohl, 2019). The intense sediment drift deposition of the late Miocene was reduced, which indicates a general decrease in bottom-water activity (Rebesco et al., 2002; Uenzelmann-Neben, 2018). The bottom-water activity shifted southward closer to the upper continental rises (e.g., Huang & Jokat, 2016; Kim et al., 2018; Uenzelmann-Neben & Gohl, 2012). Along the continental slope of East Antarctica, mass transport deposits were common along with the development of channel-levee systems, possibly related to meltwater pulses and fast deglaciation (Cooper & O'Brien, 1998; Huang & Jokat, 2016; Kuvaas & Leitchenkov, 1992) (Close, 2010; De Santis et al., 1999; Donda et al., 2008; Kim et al., 2018).

4.5. Pleistocene: A Cold-Based Antarctic Ice Sheet

The Pleistocene is characterized by further development into a polar-dominated climate with permanent ice sheets on both poles (Figure 5). The constant waxing and waning of the ice sheets across the continental shelves resulted in erosion of older strata in inner to middle shelf regions and a continuous build-up of progradational sequences on the outer shelf. The paleobathymetry of this period (0.65 Ma; Figure 10i) approaches the modern bathymetry (Figure 1). Today's main glacial outlet systems were well established, although sedimentation rates decreased in comparison to the Pliocene most likely due to the prevalence of more cold-based ice on the continent (DeConto & Pollard, 2016; Levy et al., 2019; Pollard & DeConto, 2019). Active channel-levee systems can be found along all Antarctic margins, delivering sediments toward the continental slope, particularly during glacial periods (Close, 2010; De Santis et al., 1999; Huang & Jokat, 2016; Uenzelmann-Neben, 2018).

5. Conclusion

We present a suite of high-resolution paleobathymetric grids of the circum-Antarctic Southern Ocean from the Eocene-Oligocene Boundary to the Pleistocene. These models include the most recent plate tectonic models of the Southern Ocean, as well as a detailed reconstruction of the offshore sedimentation. Our consistent, Southern Ocean-wide sedimentation model was built through reevaluating all available seismic reflection data, drill records, as well as established and newly derived seismic stratigraphies between the conjugate continental margins. The computed sediment rates and volumes show considerable variations through time and across regions and outlet glaciers, providing clues on changing past cryosphere and ocean current processes through time.

The entire suite of grids encompasses the transition from isolated ocean basins to deep-water exchange between interconnected Southern Ocean basins, the establishment and modes of the intensity of sediment transport by the ACC, the varying transport of sediments by waxing and waning of the Antarctic ice sheets, as well as the periods of the recovering of the ice sheets after warm periods.

The earliest presented time slice (Eocene-Oligocene Boundary) shows isolated basins within the Southern Ocean with the potential of limited deep-water exchange through the Southern Ocean gateways. Reformed sedimentation patterns within the Oligocene with the onset of drift deposits along the Antarctic continental rises are associated with the establishment of the ACC and the onset of stronger bottom currents throughout the Southern Ocean.

Since the onset of glaciation, sedimentation offshore Antarctica has been located in similar broad depositional areas. However, especially in East Antarctica, changes are observed in the dominance of individual

glacial outlets. For instance, the Totten glacier, one of today's main regional outlets only gains importance after the complete transition into full glacial conditions during the late Miocene.

We observe two main phases of glacial deposition in the Southern Ocean which are related to the first occurrence of the continental ice sheet in the early Oligocene and during the late Miocene after the reestablishment of full glacial conditions after the Mid-Miocene Climatic Optimum. Submarine-based portions of both ice sheets recover slower back to full glacial conditions. After the Miocene, sedimentation patterns concentrate along the shelf edges, leading to shelf progradation that enlarged the Antarctic continental shelves toward our modern bathymetry.

Data Availability Statement

The computed paleobathymetry grids as well as the sediment thickness grids are available to the community on the www.pangaea.de or under <https://doi.org/10.1594/PANGAEA.918663>.

Acknowledgments

The authors thank the numerous scientists, technicians, and ship crews involved in the acquisition and processing of the seismic reflection data as well as the data curators at OGS Trieste for providing their services within the SCAR Antarctic Seismic Data Library System (SDL). Additional data have been provided by Geoscience Australia, Spectrum Geo Ltd. This project has been funded by the Deutsche Forschungsgemeinschaft (DFG) under Projects GO724/15-1 and GO724/-2, and institutional resources from the Research Program PACES-II, Workpackage 3.2, of the Alfred Wegener Institute. The project contributes to the SCAR Scientific Research Program "Past Antarctic Ice Sheet Dynamics" (PAIS). I.S. was supported under the Australian Research Council's Special Research Initiative for Antarctic Gateway Partnership (Project ID SR140300001). K.H. further acknowledges the "Visiting Scholarship" scheme of the University of Tasmania, funding a 3-month research visit at the University of Tasmania. J.M.W. acknowledges funding from the Australian Research Council DP180102280. B.W.D. acknowledges funding support from the New Zealand MBIE for the Zealandia research programme. G.L. acknowledges the Russian Science Foundation Grant 16-17-10139. The authors would like to thank Emerson E&P Software, Emerson Automation Solutions, for providing licenses for the seismic software Paradigm in the scope of the Emerson Academic Program. The authors thank two anonymous reviewers for their enthusiastic and helpful comments, which improved the manuscript and the Pangaea data editors for their help with the publication of the paleobathymetric and isopach data sets.

References

- Aitken, A., Young, D. A., Ferraccioli, F., Betts, P. G., Greenbaum, S., Richter, T. G., et al. (2014). The subglacial geology of Wilkes Land, East Antarctica. *Paleoceanography*, *41*, 2390–2400. <https://doi.org/10.1002/2014GL059405>
- Anagnostou, E., John, E. H., Edgar, K. M., Foster, G. L., Ridgwell, A., Inglis, G. N., et al. (2016). Changing atmospheric CO₂ concentration was the primary driver of early Cenozoic climate. *Nature*, *533*(7603), 380–384. <https://doi.org/10.1038/nature17423>
- Assmann, K. M., Jenkins, A., Shoosmith, D. R., Walker, D. P., Jacobs, S. S., & Nicholls, K. W. (2013). Variability of circumpolar deep water transport onto the Amundsen Sea continental shelf through a shelf break trough. *Journal of Geophysical Research: Oceans*, *118*, 6603–6620. <https://doi.org/10.1002/2013JC008871>
- Baatsen, M., van Hinsbergen, D. J. J., von der Heydt, A. S., Dijkstra, H. A., Sluijs, A., Abels, H. A., & Bijl, P. K. (2016). Reconstructing geographical boundary conditions for palaeoclimate modelling during the Cenozoic. *Climate of the Past*, *12*(8), 1635–1644. <https://doi.org/10.5194/cp-12-1635-2016>
- Baatsen, M. L. J., von der Heydt, A. S., Kliphuis, M., Viebahn, J., & Dijkstra, H. A. (2018). Multiple states in the late Eocene ocean circulation. *Global and Planetary Change*, *163*, 18–28. <https://doi.org/10.1016/j.gloplacha.2018.02.009>
- Barker, P. F., & Thomas, E. (2004). Origin, signature and palaeoclimatic influence of the Antarctic Circumpolar Current. *Earth-Science Reviews*. <https://doi.org/10.1016/j.earscirev.2003.10.003>
- Bart, P. J. (2003). Were West Antarctic ice sheet grounding events in the Ross Sea a consequence of East Antarctic ice sheet expansion during the middle Miocene? *Earth and Planetary Science Letters*, *216*(1–2), 93–107. [https://doi.org/10.1016/S0012-821X\(03\)00509-0](https://doi.org/10.1016/S0012-821X(03)00509-0)
- Bijl, P. K., Bendle, J., & Bohaty, S. M. (2013). Eocene cooling linked to early flow across the Tasmanian Gateway. *PNAS*. <https://doi.org/10.1073/pnas.1220872110/-/DCSupplemental/pnas.201220872SI.pdf>
- Bradshaw, B. E. (2005). Geology and petroleum potential of the Bremer sub-basin, offshore southwestern Australia. *Record Geoscience Australia*, *2005*(21), 1–131.
- Brown, B., Gaina, C., & Müller, R. D. (2006). Circum-Antarctic palaeobathymetry: Illustrated examples from Cenozoic to recent times. *Palaeogeography, Palaeogeography, Palaeoecology*. <https://doi.org/10.1016/j.palaeo.2005.07.033>
- Cande, S. C., & Stock, J. M. (2004). Cenozoic reconstructions of the Australia-New Zealand-South Pacific sector of Antarctica. In *The Cenozoic Southern Ocean: Tectonics, Sedimentation, and Climate Change Between Australia and Antarctica* (Vol. 151, pp. 5–17). Washington, D. C: American Geophysical Union.
- Carter, A., Riley, T. R., Hillenbrand, C.-D., & Rittner, M. (2017). Widespread Antarctic glaciation during the Late Eocene. *Earth and Planetary Science Letters*, *458*, 49–57. <https://doi.org/10.1016/j.epsl.2016.10.045>
- Castelino, J. A., Eagles, G., & Jokat, W. (2016). Anomalous bathymetry and palaeobathymetric models of the Mozambique Basin and Riiser Larsen Sea. *Earth and Planetary Science Letters*, *455*, 25–37. <https://doi.org/10.1016/j.epsl.2016.09.018>
- Charvis, P., & Operto, S. (1999). Structure of the Cretaceous Kerguelen Volcanic Province (southern Indian Ocean) from wide-angle seismic data. *Journal of Geodynamics*, *28*(1), 51–71. [https://doi.org/10.1016/S0264-3707\(98\)00029-5](https://doi.org/10.1016/S0264-3707(98)00029-5)
- Close, D. I. (2010). Slope and fan deposition in deep-water turbidite systems, East Antarctica. *Marine Geology*, *274*(1–4), 21–31. <https://doi.org/10.1016/j.margeo.2010.03.002>
- Close, D. I., Stagg, H., & O'Brien, P. E. (2007). Seismic stratigraphy and sediment distribution on the Wilkes Land and Terre Adélie margins, East Antarctica. *Marine Geology*, *239*(1–2), 33–57. <https://doi.org/10.1016/j.margeo.2006.12.010>
- Colleoni, F., de Santis, L., Montoli, E., Olivo, E., Sorlien, C. C., Bart, P. J., et al. (2018). Past continental shelf evolution increased Antarctic ice sheet sensitivity to climatic conditions. *Scientific Reports*, *8*(1), 1–12. <https://doi.org/10.1038/s41598-018-29718-7>
- Colleoni, F., De Santis, L., Siddoway, C. S., Bergamasco, A., Golledge, N. R., Lohmann, G., et al. (2018). Spatio-temporal variability of processes across Antarctic ice-bed-ocean interfaces. *Nature Communications*, *9*(1), 2289. <https://doi.org/10.1038/s41467-018-04583-0>
- Cooper, A., & O'Brien, P. (1998). 1. Leg 188 Synthesis: Transitions in the glacial history of the Prydz Bay region, East Antarctica, from ODP drilling. *Proceeding of the Ocean Drilling Program, Scientific Results*, *188*, 1–42.
- Cramer, B. S., Toggweiler, J. R., Wright, J. D., Katz, M. E., & Miller, K. G. (2009). Ocean overturning since the Late Cretaceous: Inferences from a new benthic foraminiferal isotope compilation. *Paleoceanography*, *24*, PA4216. <https://doi.org/10.1029/2008PA001683>
- De Santis, L., Brancolini, G., & Donda, F. (2003). Seismo-stratigraphic analysis of the Wilkes Land continental margin (East Antarctica): Influence of glacially driven processes on the Cenozoic deposition. *Deep Sea Research Part II: Topical Studies in Oceanography*, *50*(8–9), 1563–1594. [https://doi.org/10.1016/S0967-0645\(03\)00079-1](https://doi.org/10.1016/S0967-0645(03)00079-1)
- De Santis, L., Prato, S., Brancolini, G., Lovato, M., & Torelli, L. (1999). The eastern Ross Sea continental shelf during the Cenozoic: Implications for the West Antarctic ice sheet development. *Global and Planetary Change*, *23*, 173–196. [https://doi.org/10.1016/S0921-8181\(99\)00056-9](https://doi.org/10.1016/S0921-8181(99)00056-9)
- DeConto, R. M., & Pollard, D. (2003). Rapid Cenozoic glaciation of Antarctica induced by declining atmospheric CO₂. *Nature*, *421*(6920), 245–249. <https://doi.org/10.1038/nature01290>

- DeConto, R. M., & Pollard, D. (2016). Contribution of Antarctica to past and future sea-level rise. *Nature*, *531*(7596), 591–597. <https://doi.org/10.1038/nature17145>
- Diekmann, B., Kuhn, G., Gersonde, R., & Mackensen, A. (2004). Middle Eocene to early Miocene environmental changes in the sub-Antarctic Southern Ocean: Evidence from biogenic and terrigenous depositional patterns at ODP Site 1090. *Global and Planetary Change*, *40*(3–4), 295–313. <https://doi.org/10.1016/j.gloplacha.2003.09.001>
- Diester-Haass, L. (1995). Middle Eocene to early Oligocene paleoceanography of the Antarctic Ocean (Maud Rise, ODP Leg 113, Site 689): Change from a low to a high productivity ocean. *Palaeogeography, Palaeoclimatology, Palaeoecology*, *113*(2–4), 311–334. [https://doi.org/10.1016/0031-0182\(95\)00067-V](https://doi.org/10.1016/0031-0182(95)00067-V)
- Donda, F., Brancolini, G., De Santis, L., & Trincardi, F. (2003). Seismic facies and sedimentary processes on the continental rise off Wilkes Land (East Antarctica): Evidence of bottom current activity. *Deep Sea Research Part II: Topical Studies in Oceanography*, *50*(8–9), 1509–1527. [https://doi.org/10.1016/S0967-0645\(03\)00075-4](https://doi.org/10.1016/S0967-0645(03)00075-4)
- Donda, F., Leitchenkov, G., Brancolini, G., Romeo, R., De Santis, L., Escutia, C., et al. (2020). The influence of Totten Glacier on the Late Cenozoic sedimentary record. *Antarctic Science*, *111*, 1–13. <https://doi.org/10.1017/S0954102020000188>
- Donda, F., O'Brien, P. E., De Santis, L., Rebesco, M., & Brancolini, G. (2008). Mass wasting processes in the Western Wilkes Land margin: Possible implications for East Antarctic glacial history. *Palaeogeography, Palaeoclimatology, Palaeoecology*, *260*(1–2), 77–91. <https://doi.org/10.1016/j.palaeo.2007.08.008>
- Dumitru, O. A., Austermann, J., Polyak, V. J., Fornós, J. J., Asmerom, Y., Ginés, J., et al. (2019). Constraints on global mean sea level during Pliocene warmth. *Nature*, *574*(7777), 233–236. <https://doi.org/10.1038/s41586-019-1543-2>
- Dutrieux, P., De Rydt, J., Jenkins, A., Holland, P. R., Ha, H. K., Lee, S. H., et al. (2014). Strong sensitivity of Pine Island ice-shelf melting to climatic variability. *Science*, *343*(6167), 174–178. <https://doi.org/10.1126/science.1244341>
- Eagles, G., & Jokat, W. (2014). Tectonic reconstructions for paleobathymetry in Drake Passage. *Tectonophysics*, *611*, 28–50. <https://doi.org/10.1016/j.tecto.2013.11.021>
- Escutia, C., Bentley, M. J., Florindo, F., & DeConto, R. M. (2012). Cenozoic evolution of Antarctic climates, oceans and ice sheets: An introduction. *Palaeogeography, Palaeoclimatology, Palaeoecology*, *335*–336(C), 1–3. <https://doi.org/10.1016/j.palaeo.2012.04.005>
- Escutia, C., Brinkhuis, H., Klaus, A., Expedition 318 Scientists (2010). Expedition 318 summary. Paper presented at Proceedings of the Integrated Ocean Drilling Program Volume 318 Expedition Reports, Integrated Ocean Drilling Program Management International, Inc., for the Integrated Ocean Drilling Program. <https://doi.org/10.2204/iodp.proc.318.101.2011>
- Escutia, C., De Santis, L., Donda, F., Dunbar, R. B., Cooper, A. K., Brancolini, G., & Eitrem, S. L. (2005). Cenozoic ice sheet history from East Antarctic Wilkes Land continental margin sediments. *Global and Planetary Change*, *45*(1–3), 51–81. <https://doi.org/10.1016/j.gloplacha.2004.09.010>
- Escutia, C., Eitrem, S. L., Cooper, A. K., & Nelson, C. H. (2000). Morphology and acoustic character of the Antarctic Wilkes Land Turbidite systems: Ice-sheet-sourced versus river-sourced fans. *Journal of Sedimentary Research*, *70*(1), 84–93. <https://doi.org/10.1306/2DC40900-0E47-11D7-8643000102C1865D>
- Finn, C. A., Müller, R. D., & Panter, K. S. (2005). A Cenozoic diffuse alkaline magmatic province (DAMP) in the southwest Pacific without rift or plume origin. *Geochemistry, Geophysics, Geosystems*, *6*, Q02005. <https://doi.org/10.1029/2004GC000723>
- Foster, G. L., Royer, D. L., & Lunt, D. J. (2017). Future climate forcing potentially without precedent in the last 420 million years. *Nature Communications*, *8*(1), 1–8. <https://doi.org/10.1038/ncomms14845>
- Francis, T. J. G., & Raitt, R. W. (1967). Seismic refraction measurements in the southern Indian Ocean. *Journal of Geophysical Research*, *72*(12), 3015–3041. <https://doi.org/10.1029/JZ072i012p03015>
- Fretwell, P., Pritchard, H. D., Vaughan, D. G., Bamber, J. L., Barrand, N. E., Bell, R., et al. (2013). Bedmap2: Improved ice bed, surface and thickness datasets for Antarctica. *Cryosphere*, *7*, 375–393. <https://doi.org/10.5194/tc7-375-2013>
- Galeotti, S., DeConto, R., Naish, T., Stocchi, P., Florindo, F., Pagani, M., et al. (2016). Antarctic ice sheet variability across the Eocene-Oligocene boundary climate transition. *Science*, *352*(6281), 76–80. <https://doi.org/10.1126/science.aab0669>
- Gasson, E., DeConto, R. M., Pollard, D., & Levy, R. (2016). Dynamic Antarctic ice sheet during the early to mid-Miocene. *PNAS*. <https://doi.org/10.1073/pnas.1516130113>
- Gohl, K. (2012). Basement control on past ice sheet dynamics in the Amundsen Sea Embayment, West Antarctica. *Palaeogeography, Palaeoclimatology, Palaeoecology*, *335*–336(C), 35–41. <https://doi.org/10.1016/j.palaeo.2011.02.022>
- Gohl, K., Denk, A., Eagles, G., & Wobbe, F. (2013). Deciphering tectonic phases of the Amundsen Sea Embayment shelf, West Antarctica, from a magnetic anomaly grid. *Tectonophysics*, *585*(C), 113–123. <https://doi.org/10.1016/j.tecto.2012.06.036>
- Gohl, K., Leitchenkov, G. L., Parsieglia, N., Ehlers, B. M., Kopsch, C., Damaske, D., et al. (2007). *Crustal types and continent-ocean boundaries between the Kerguelen Plateau and Prydz Bay, East Antarctica* (pp. 1–4). Paper presented at Antarctica: A Keystone in a Changing World-Online Proceedings of the 10th ISAES X, USGS Open-File Report 2007-1047, Extended Abstract 038.
- Gohl, K., & Uenzelmann-Neben, G. (2001). The crustal role of the Agulhas Plateau, southwest Indian Ocean: Evidence from seismic profiling. *Geophysical Journal International*, *144*(3), 632–646. <https://doi.org/10.1046/j.1365-246X.2001.01368.x>
- Gohl, K., Uenzelmann-Neben, G., & Grobys, N. (2011). Growth and dispersal of a Southeast African large igneous province. *South African Journal of Geology*. <https://doi.org/10.2113/gssajg.114.3-4.379>
- Gohl, K., Uenzelmann-Neben, G., Larter, R. D., Hillenbrand, C.-D., Hochmuth, K., Kalberg, T., et al. (2013). Seismic stratigraphic record of the Amundsen Sea Embayment shelf from pre-glacial to recent times: Evidence for a dynamic West Antarctic ice sheet. *Marine Geology*, *344*, 115–131. <https://doi.org/10.1016/j.margeo.2013.06.011>
- Gruetner, J., & Uenzelmann-Neben, G. (2016). Contourite drifts as indicators of Cenozoic bottom water intensity in the eastern Agulhas ridge area, South Atlantic. *Marine Geology*, *378*(C), 350–360. <https://doi.org/10.1016/j.margeo.2015.12.003>
- Gulick, S. P. S., Shevenell, A. E., Montelli, A., Fernandez, R., Smith, C., Warny, S., et al. (2017). Initiation and long-term instability of the East Antarctic ice sheet. *Nature*, *552*(7684), 225–229. <https://doi.org/10.1038/nature25026>
- Hayes, D. E., Zhang, C., & Weissel, R. A. (2009). Modeling Paleobathymetry in the Southern Ocean. *Eos Transactions American Geophysical Union*, *90*(19), 165–166. <https://doi.org/10.1029/2009EO190001>
- Hochmuth, K., & Gohl, K. (2013). Glaciomarine sedimentation dynamics of the Abbot glacial trough of the Amundsen Sea Embayment shelf, West Antarctica. *Geological Society, London, Special Publications*, *381*(1), 233–244. <https://doi.org/10.1144/SP381.21>
- Hochmuth, K., & Gohl, K. (2019). Seaward growth of Antarctic continental shelves since establishment of a continent-wide ice sheet: Patterns and mechanisms. *Palaeogeography, Palaeoclimatology, Palaeoecology*, *520*, 44–54. <https://doi.org/10.1016/j.palaeo.2019.01.025>
- Horn, M., & Uenzelmann-Neben, G. (2015). The Deep Western Boundary Current at the Bounty Trough, east of New Zealand: Indications for its activity already before the opening of the Tasmanian Gateway. *Marine Geology*, *362*, 60–75. <https://doi.org/10.1016/j.margeo.2015.01.011>

- Huang, X., Gohl, K., & Jokat, W. (2014). Variability in Cenozoic sedimentation and paleo-water depths of the Weddell Sea basin related to pre-glacial and glacial conditions of Antarctica. *Global and Planetary Change*, *118*, 25–41. <https://doi.org/10.1016/j.gloplacha.2014.03.010>
- Huang, X., & Jokat, W. (2016). Middle Miocene to present sediment transport and deposits in the Southeastern Weddell Sea, Antarctica. *Global and Planetary Change*, *139*(C), 211–225. <https://doi.org/10.1016/j.gloplacha.2016.03.002>
- Huang, X., Stärz, M., Gohl, K., Knorr, G., & Lohmann, G. (2017). Impact of Weddell Sea shelf progradation on Antarctic bottom water formation during the Miocene. *Paleoceanography*, *32*, 304–317. <https://doi.org/10.1002/2016PA002987>
- Ito, G., & Clift, P. D. (1998). Subsidence and growth of Pacific Cretaceous plateaus. *Earth and Planetary Science Letters*, *161*, 85–100.
- Jokat, W., & Herter, U. (2016). Jurassic failed rift system below the Filchner-Ronne-Shelf, Antarctica: New evidence from geophysical data. *Tectonophysics*, *688*(C), 65–83. <https://doi.org/10.1016/j.tecto.2016.09.018>
- Jokat, W., Ritzmann, O., Reichert, C., & Hinz, K. (2004). Deep crustal structure of the continental margin off the Explora Escarpment and in the Lazarev Sea, East Antarctica. *Marine Geophysical Researches*, *25*(3–4), 283–304. <https://doi.org/10.1007/s11001-005-1337-9>
- Kennett, J. P. (1977). Cenozoic evolution of Antarctic glaciation, the circum-Antarctic Ocean, and their impact on global paleoceanography. *Journal of Geophysical Research*. <https://doi.org/10.1029/JC082i027p03843>
- Kim, S., de Santis, L., Hong, J. K., Cottlerle, D., Petronio, L., Colizza, E., et al. (2018). Seismic stratigraphy of the Central Basin in north-western Ross Sea slope and rise, Antarctica: Clues to the late Cenozoic ice-sheet dynamics and bottom-current activity. *Marine Geology*, *395*, 363–379. <https://doi.org/10.1016/j.margeo.2017.10.013>
- Kipf, A., Hauff, F., Werner, R., Gohl, K., van den Bogaard, P., Hoernle, K., et al. (2014). Gondwana research. *Gondwana Research*, *25*(4), 1660–1679. <https://doi.org/10.1016/j.gr.2013.06.013>
- Kulhanek, D. K., Levy, R. H., Clowes, C. D., Prebble, J. G., Rodelli, D., Jovane, L., et al. (2019). Revised chronostratigraphy of DSDP Site 270 and late Oligocene to early Miocene paleoecology of the Ross Sea sector of Antarctica. *Global and Planetary Change*, *178*, 46–64. <https://doi.org/10.1016/j.gloplacha.2019.04.002>
- Kuvaas, B., Kristoffersen, Y., Guseva, J., Leitchenkov, G., Gandjukhin, V., & Kudryavtsev, G. (2005). Input of glaciomarine sediments along the East Antarctic continental margin; depositional processes on the Cosmonaut Sea continental slope and rise and a regional acoustic stratigraphic correlation from 40 °W to 80 °E. *Marine Geophysical Researches*, *25*(3–4), 247–263. <https://doi.org/10.1007/s11001-005-1321-4>
- Kuvaas, B., & Leitchenkov, G. (1992). Glaciomarine turbidite and current controlled deposits in Prydz Bay, Antarctica. *Journal of Applied Geophysics*, *108*, 365–381. [https://doi.org/10.1016/0025-3227\(92\)90205](https://doi.org/10.1016/0025-3227(92)90205)
- LaCasce, J. H., Escartin, J., Chassignet, E. P., & Xu, X. (2019). Jet instability over smooth, corrugated, and realistic bathymetry. *Journal of Physical Oceanography*, *49*(2), 585–605. <https://doi.org/10.1175/JPO-D-18-0129.1>
- Larter, R. D., Cunningham, A., Barker, P., Gohl, K., & Nitsche, F. O. (2002). Tectonic evolution of the Pacific margin of Antarctica 1. Late Cretaceous tectonic reconstructions. *Journal of Geophysical Research*, *107*(B12), 2345. <https://doi.org/10.1029/2000JB000052>
- Leckie, R. M., & Webb, P. N. (1983). Late Oligocene–early Miocene glacial record of the Ross Sea, Antarctica: Evidence from DSDP site 270. *Geology*, *11*(10), 578. [https://doi.org/10.1130/0091-7613\(1983\)11<578:LOMGRO>2.0.CO;2](https://doi.org/10.1130/0091-7613(1983)11<578:LOMGRO>2.0.CO;2)
- Leitchenkov, G., Guseva, J., Gandjukhin, V., Griukurov, G., Kristoffersen, Y., Sand, M., et al. (2008). Crustal structure and tectonic provinces of the Riiser-Larsen Sea area (East Antarctica): Results of geophysical studies. *Marine Geophysical Researches*, *29*(2), 135–158. <https://doi.org/10.1007/s11001-008-9051-z>
- Leitchenkov, G. L., Guseva, Y. B., & Gandjukhin, V. V. (2007). *Cenozoic environmental changes along the East Antarctic continental margin inferred from regional seismic stratigraphy* (pp. 1–4). Paper presented at Antarctica: A Keystone in a Changing World—Online Proceedings of the 10th ISAES, USGS Open-File Report 2007–1047, Short Research Paper 005. <https://doi.org/10.3133/ofr20071047SRP005>
- Levy, R. H., Meyers, S. R., Naish, T. R., Gollledge, N. R., McKay, R. M., Crampton, J. S., et al. (2019). Antarctic ice-sheet sensitivity to obliquity forcing enhanced through ocean connections. *Nature Geoscience*, *12*(2), 132–137. <https://doi.org/10.1038/s41561-018-0284-4>
- Lindeque, A., Gohl, K., Henrys, S., Wobbe, F., & Davy, B. (2016). Seismic stratigraphy along the Amundsen Sea to Ross Sea continental rise: A cross-regional record of pre-glacial to glacial processes of the West Antarctic margin. *Palaeogeography, Palaeoclimatology, Palaeoecology*, *443*, 183–202. <https://doi.org/10.1016/j.palaeo.2015.11.017>
- Lindeque, A., Gohl, K., Wobbe, F., & Uenzelmann-Neben, G. (2016). Preglacial to glacial sediment thickness grids for the Southern Pacific Margin of West Antarctica. *Geochemistry, Geophysics, Geosystems*, *17*, 4276–4285. <https://doi.org/10.1002/2016GC006401>
- Liu, Z., Pagani, M., Zinniker, D., DeConto, R., Huber, M., Brinkhuis, H., et al. (2009). Global cooling during the Eocene-Oligocene climate transition. *Science*, *323*(5918), 1187–1190. <https://doi.org/10.1126/science.1166368>
- Lowe, A. L., & Anderson, J. B. (2002). Reconstruction of the West Antarctic ice sheet in Pine Island Bay during the Last Glacial Maximum and its subsequent retreat history. *Quaternary Science Reviews*, *21*(16–17), 1879–1897. [https://doi.org/10.1016/S0277-3791\(02\)00006-9](https://doi.org/10.1016/S0277-3791(02)00006-9)
- McKenzie, D. (1978). Some remarks on the development of sedimentary basins. *Earth and Planetary Science Letters*, *40*, 25–32.
- Müller, R. D., Cannon, J., Qin, X., Watson, R. J., Gurnis, M., Williams, S., et al. (2018). GPlates: Building a virtual Earth through deep time. *Geochemistry, Geophysics, Geosystems*, *19*, 2243–2261. <https://doi.org/10.1029/2018GC007584>
- Müller, R. D., Seton, M., Zahirovic, S., Williams, S. E., Matthews, K. J., Wright, N. M., et al. (2016). Ocean Basin evolution and global-scale plate reorganization events since Pangea breakup. *Annual Review of Earth and Planetary Sciences*, *44*(1), 107–138. <https://doi.org/10.1146/annurev-earth-060115-012211>
- Nakayama, Y., Menemenlis, D., Schodlok, M., & Rignot, E. (2017). Amundsen and Bellingshausen Seas simulation with optimized ocean, sea ice, and thermodynamic ice shelf model parameters. *Journal of Geophysical Research: Oceans*, *122*, 6180–6195. <https://doi.org/10.1002/2016JC012538>
- Nitsche, F. O., Cunningham, A. P., Larter, R. D., & Gohl, K. (2000). Geometry and development of glacial continental margin depositional systems in the Bellingshausen Sea. *Marine Geology*, *162*(2–4), 277–302.
- O'Brien, P. E., et al. (2004). Prydz Channel Fan and the history of extreme ice advances in Prydz Bay. *Proceeding of the Ocean Drilling Program, Scientific Results*, *188*.
- Pagani, M., Zachos, J. C., Freeman, K. H., Tipple, B., & Bohaty, S. (2005). Marked decline in atmospheric carbon dioxide concentrations during the Paleogene. *Science*, *309*(5734), 600–603. <https://doi.org/10.1126/science.1110063>
- Parsiegla, N., Gohl, K., & Uenzelmann-Neben, G. (2008). The Agulhas Plateau: Structure and evolution of a large igneous province. *Geophysical Journal International*, *174*(1), 336–350. <https://doi.org/10.1111/j.1365-246X.2008.03808.x>
- Passchier, S., Ciarletta, D. J., Henao, V., & Sekkas, V. (2019). Sedimentary processes and facies on a high-latitude passive continental margin, Wilkes Land, East Antarctica. *Geological Society, London, Special Publications*, *475*(1), 181–201. <https://doi.org/10.1144/SP475.3>

- Passchier, S., Ciarletta, D. J., Miriagos, T. E., Bijl, P. K., & Bohaty, S. M. (2017). An Antarctic stratigraphic record of stepwise ice growth through the Eocene-Oligocene transition. *Geological Society of America Bulletin*, *129*(3–4), 318–330. <https://doi.org/10.1130/B31482.1>
- Paxman, G. J. G., Jamieson, S. S. R., Ferraccioli, F., Bentley, M. J., Ross, N., Armadillo, E., et al. (2018). Bedrock erosion surfaces record former East Antarctic ice sheet extent. *Geophysical Research Letters*, *45*, 4114–4123. <https://doi.org/10.1029/2018GL077268>
- Paxman, G. J. G., Jamieson, S. S. R., Hochmuth, K., Gohl, K., Bentley, M. J., Leitchenkov, G., & Ferraccioli, F. (2019). Reconstructions of Antarctic topography since the Eocene–Oligocene boundary. *Palaeogeography, Palaeoclimatology, Palaeoecology*, *535*, 109346. <https://doi.org/10.1016/j.palaeo.2019.109346>
- Pearson, P. N., Foster, G. L., & Wade, B. S. (2009). Atmospheric carbon dioxide through the Eocene-Oligocene climate transition. *Nature*, *461*(7267), 1110–1113. <https://doi.org/10.1038/nature08447>
- Pollard, D., & DeConto, R. M. (2019). Continuous simulations over the last 40 million years with a coupled Antarctic ice sheet-sediment model. *Palaeogeography, Palaeoclimatology, Palaeoecology*, *535*, 374–47. <https://doi.org/10.1016/j.palaeo.2019.109374>
- Powell, R. D., & Cooper, J. M. (2002). A glacial sequence stratigraphic model for temperate, glaciated continental shelves. *Geological Society, London, Special Publications*, *203*(1), 215–244. <https://doi.org/10.1144/GSL.SP.2002.203.01.12>
- Pritchard, H. D., Ligtenberg, S. R. M., Fricker, H. A., Vaughan, D. G., van den Broeke, M. R., & Padman, L. (2012). Antarctic ice-sheet loss driven by basal melting of ice shelves. *Nature*, *484*(7395), 502–505. <https://doi.org/10.1038/nature10968>
- Raymond, C. A., LaBrecque, J., & Kristoffersen, Y. (1991). Islas Orcadas Rise and Meteor Rise: The tectonic and depositional history of two aseismic plateaus from Sites 702, 703, and 704. *Proceeding of the Ocean Drilling Program, Scientific Results*, *114*.
- Rebesco, M., Larter, R. D., Camerlenghi, A., & Barker, P. F. (1996). Giant sediment drifts on the continental rise west of the Antarctic Peninsula. *Geo-Marine Letters*, *16*(2), 65–75. <https://doi.org/10.1007/BF02202600>
- Rebesco, M., Pudsey, C. J., Canals, M., Camerlenghi, A., Barker, P. F., Estrada, F., & Giorgetti, A. (2002). Sediment drifts and deep-sea channel systems, Antarctic Peninsula Pacific Margin. *Geological Society, London, Memoirs*, *22*(1), 353–371.
- Recq, M., Goslin, J., Charvis, P., & Operto, S. (1998). Small-scale crustal variability within an intraplate structure: The Crozet Bank (southern Indian Ocean). *Geophysical Journal International*, *134*(1), 145–156. <https://doi.org/10.1046/j.1365-246x.1998.00530.x>
- Richards, F. D., Hoggard, M. J., Cowton, L. R., & White, N. J. (2018). Reassessing the thermal structure of oceanic lithosphere with revised global inventories of basement depths and heat flow measurements. *Journal of Geophysical Research: Solid Earth*, *123*, 9136–9161. <https://doi.org/10.1029/2018JB015998>
- Rignot, E., Bamber, J. L., van den Broeke, M. R., Davis, C., Li, Y., van de Berg, W. J., & van Meijgaard, E. (2008). Recent Antarctic ice mass loss from radar interferometry and regional climate modelling. *Nature Geoscience*, *1*(2), 106–110. <https://doi.org/10.1038/ngeo102>
- Sangiorgi, F., Bijl, P. K., Passchier, S., Salzmann, U., Schouten, S., McKay, R., et al. (2018). Southern Ocean warming and Wilkes Land ice sheet retreat during the mid-Miocene. *Nature Communications*, *9*(1), 1–11. <https://doi.org/10.1038/s41467-017-02609-7>
- Sauermilch, I., Mateo, Z. R. P., & Boaga, J. (2019). A comparative analysis of time–depth relationships derived from scientific ocean drilling expeditions. *Marine Geophysical Researches*, *40*(4), 635–641. <https://doi.org/10.1007/s11001-019-09393-7>
- Sauermilch, I., Whittaker, J. M., Bijl, P. K., Totterdell, J. M., & Jokat, W. (2019). Tectonic, oceanographic, and climatic controls on the Cretaceous-Cenozoic sedimentary record of the Australian-Antarctic Basin. *Journal of Geophysical Research: Solid Earth*, *124*, 7699–7724. <https://doi.org/10.1029/2018JB016683>
- Scher, H. D., Whittaker, J. M., Williams, S. E., Latimer, J. C., Kordesch, W. E. C., & Delaney, M. L. (2015). Onset of Antarctic Circumpolar Current 30 million years ago as Tasmanian Gateway aligned with westerlies. *Nature*, *523*(7562), 580–583. <https://doi.org/10.1038/nature14598>
- Scheuer, C., Gohl, K., & Eagles, G. (2006). Gridded isopach maps from the South Pacific and their use in interpreting the sedimentation history of the West Antarctic continental margin. *Geochemistry, Geophysics, Geosystems*, *7*, Q11015. <https://doi.org/10.1029/2006GC001315>
- Schodlok, M. P., Menemenlis, D., Rignot, E., & Studinger, M. (2017). Sensitivity of the ice-shelf/ocean system to the sub-ice-shelf cavity shape measured by NASA IceBridge in Pine Island Glacier, West Antarctica. *Annals of Glaciology*, *53*(60), 156–162. <https://doi.org/10.3189/2012AoG60A073>
- Seton, M., Müller, R. D., Zahirovic, S., Gaina, C., Torsvik, T., Shephard, G., et al. (2012). Global continental and ocean basin reconstructions since 200Ma. *Earth-Science Reviews*, *113*(3–4), 212–270. <https://doi.org/10.1016/j.earscirev.2012.03.002>
- Smith, R. T., & Anderson, J. B. (2010). Ice-sheet evolution in James Ross Basin, Weddell Sea margin of the Antarctic Peninsula: The seismic stratigraphic record. *Geological Society of America Bulletin*, *122*(5–6), 830–842. <https://doi.org/10.1130/B26486.1>
- Solli, K., Kuvaas, B., Kristoffersen, Y., Leitchenkov, G., Guseva, J., & Gandjukhin, V. (2007). A seismic-stratigraphic analysis of glacio-marine deposits in the eastern Riiser-Larsen Sea (Antarctica). *Marine Geophysical Researches*, *28*(1), 43–57. <https://doi.org/10.1007/s11001-007-9013-x>
- Spiegel, C., Lindow, J., Kamp, P. J. J., Meisel, O., Mukasa, S., Lisker, F., et al. (2016). Tectonomorphic evolution of Marie Byrd Land—Implications for Cenozoic rifting activity and onset of West Antarctic glaciation. *Global and Planetary Change*, *145*(C), 98–115. <https://doi.org/10.1016/j.gloplacha.2016.08.013>
- Stacey, A., Mitchell, C., Struckmeyer, H. I. M., & Totterdell, J. (2013). *Geology and hydrocarbon prospectivity of the deepwater Otway and Sorell basins, offshore southeastern Australia (Record 2013/02)*. Geoscience Australia: Canberra.
- Stagg, H. (1985). The structure and origin of Prydz Bay and MacRobertson shelf, East Antarctica. *Tectonophysics*, *114*(1–4), 315–340. [https://doi.org/10.1016/0040-1951\(85\)90019-8](https://doi.org/10.1016/0040-1951(85)90019-8)
- Stein, C. A., & Stein, S. (1992). A model for the global variation in oceanic depth and heat flow with lithospheric age. *Nature*, *359*(6391), 123–129.
- Straume, E. O., Gaina, C., Medvedev, S., Hochmuth, K., Gohl, K., Whittaker, J. M., et al. (2019). GlobSed: Updated total sediment thickness in the world's oceans. *Geochemistry, Geophysics, Geosystems*, *20*, 1756–1772. <https://doi.org/10.1029/2018GC008115>
- Totterdell, J. M., Blevin, J. E., Struckmeyer, H. I. M., Bradshaw, B. E., Colwell, J. B., & Kennard, J. M. (2000). A new sequence framework for the Great Australian Bight: Starting with a clean slate. *The APPEA Journal*, *40*(1), 95–118. <https://doi.org/10.1071/aj99007>
- Uenzelmann-Neben, G. (2006). Depositional patterns at Drift 7, Antarctic Peninsula: Along-slope versus down-slope sediment transport as indicators for oceanic currents and climatic conditions. *Marine Geology*, *233*(1–4), 49–62. <https://doi.org/10.1016/j.margeo.2006.08.008>
- Uenzelmann-Neben, G. (2018). Variations in ice-sheet dynamics along the Amundsen Sea and Bellingshausen Sea West Antarctic ice sheet margin. *Geological Society of America Bulletin*. <https://doi.org/10.1130/B31744.1>
- Uenzelmann-Neben, G., & Gohl, K. (2012). Amundsen Sea sediment drifts: Archives of modifications in oceanographic and climatic conditions. *Marine Geology*, *299*–302, 51–62. <https://doi.org/10.1016/j.margeo.2011.12.007>

- Uenzelmann-Neben, G., & Gohl, K. (2014). Early glaciation already during the Early Miocene in the Amundsen Sea, Southern Pacific: Indications from the distribution of sedimentary sequences. *Global and Planetary Change*, *120*, 92–104. <https://doi.org/10.1016/j.gloplacha.2014.06.004>
- Uenzelmann-Neben, G., & Huhn, K. (2009). Sedimentary deposits on the southern South African continental margin: Slumping versus non-deposition or erosion by oceanic currents? *Marine Geology*, *266*(1–4), 65–79. <https://doi.org/10.1016/j.margeo.2009.07.011>
- van Hinsbergen, D. J. J., de Groot, L. V., van Schaik, S. J., Spakman, W., Bijl, P. K., Sluijs, A., et al. (2015). A paleolatitude calculator for paleoclimate studies, edited by D. L. Royer. *PLOS ONE*, *10*(6), e0126946–e0126921. <https://doi.org/10.1371/journal.pone.0126946>
- van Wyk de Vries, M., Bingham, R. G., & Hein, A. S. (2018). A new volcanic province: An inventory of subglacial volcanoes in West Antarctica. *Geological Society, London, Special Publications*, *461*(1), 231–248. <https://doi.org/10.1144/SP461.7>
- Viebahn, J. P., von der Heydt, A. S., Le Bars, D., & Dijkstra, H. A. (2016). Effects of Drake Passage on a strongly eddying global ocean. *Paleoceanography*, *31*, 564–581. <https://doi.org/10.1002/2015PA002888>
- Villa, G., Fioroni, C., Persico, D., Roberts, A. P., & Florindo, F. (2014). Middle Eocene to Late Oligocene Antarctic glaciation/deglaciation and southern ocean productivity. *Paleoceanography*, *29*, 223–237. <https://doi.org/10.1002/2013PA002518>
- Weatherall, P., Marks, K. M., Jakobsson, M., Schmitt, T., Tani, S., Arndt, J.-E., et al. (2015). A new digital bathymetric model of the world's oceans. *Earth and Space Science*, *2*, 331–345. <https://doi.org/10.1002/2015EA000107>
- White, R. S., McKenzie, D., & O'Nions, R. K. (1992). Oceanic crustal thickness from seismic measurements and rare earth element inversions. *Journal of Geophysical Research*, *97*(B13), 19683–19715.
- Whittaker, J. M., Goncharov, A., Williams, S. E., Müller, R. D., & Leitchkov, G. (2013). Global sediment thickness data set updated for the Australian-Antarctic Southern Ocean. *Geochemistry, Geophysics, Geosystems*, *14*, 3297–3305. <https://doi.org/10.1002/ggge.20181>
- Whittaker, J. M., Müller, R. D., Leitchkov, G., Stagg, H., Sdrolias, M., Gaina, C., & Goncharov, A. (2007). Major Australian-Antarctic plate reorganization at Hawaiian-emperor bend time. *Science*, *318*(5847), 83–86. <https://doi.org/10.1126/science.1143769>
- Whittaker, J. M., Williams, S. E., & Müller, R. D. (2013). Revised tectonic evolution of the Eastern Indian Ocean. *Geochemistry, Geophysics, Geosystems*, *14*, 1891–1909. <https://doi.org/10.1002/ggge.20120>
- Wilson, D. S., Jamieson, S. S. R., Barrett, P. J., Leitchkov, G., Gohl, K., & Larter, R. D. (2012). Antarctic topography at the Eocene–Oligocene boundary. *Palaeogeography, Palaeoclimatology, Palaeoecology*, *335–336*, 24–34. <https://doi.org/10.1016/j.palaeo.2011.05.028>
- Wobbe, F., Gohl, K., Chambord, A., & Sutherland, R. (2012). Structure and breakup history of the rifted margin of West Antarctica in relation to Cretaceous separation from Zealandia and Bellingshausen plate motion. *Geochemistry, Geophysics, Geosystems*, *13*, Q04W12. <https://doi.org/10.1029/2011GC003742>
- Wold, C. N. (1995). Palaeobathymetric reconstruction on a gridded database: The northern North Atlantic and southern Greenland-Iceland-Norwegian sea. *Geological Society, London, Special Publications*, *90*(1), 271–302. <https://doi.org/10.1144/GSL.SP.1995.090.01.17>
- Zachos, J. C., Dickens, G. R., & Zeebe, R. E. (2008). An early Cenozoic perspective on greenhouse warming and carbon-cycle dynamics. *Nature*, *451*(7176), 279–283. <https://doi.org/10.1038/nature06588>